Review 1 Comments and Responses: Comments are in black and responses are in red

This paper describes autumn-winter measurements within an Antarctic polynya during katabatic wind events. These data have been collected in extraordinarily unpleasant conditions and the authors are to be complemented on the number and quality of their measurements. Given the time and place and circumstances under which they were collected, such data are unique and valuable. This paper contributes to our scientific understanding of these important, but rarely observed, katabatic events, making direct observations of how ice formation takes place in these violent conditions. The authors add value by comparing their in situ measurements to those derived from other sources (model, satellite etc).

However I have a number of comments regarding the presentation of the data which I elaborate on below.

Comment 1: The notation used in the equations and particularly in the supplementary material are not consistent throughout the paper, leading to confusion. For example line 400 states that the total mass of frazil is MassSice. However line 81 of Supplemental states that the total mass of frazil is MassTwai. Some work is required to please ensure consistency of definitions of symbols throughout the Supplementals and the main body of the text.

Thank you, all equations have been fixed and reviewed for internal consistency.

Comment 2: Is it important that the stations retain their station number from the field campaign? It would be easier for the reader to see patterns in the tables and Figure 10 if there was a simple and intuitive ordering of station numbers, say from the coast outwards.

We recognize that a sequential numbering system for the stations would be more logical. However, we also think there is a lot of value in being able to relate these data back to the hydrographic data that is stored in the public domain. For this reason, we argue that it is worthwhile to retain the original numbering so that they would match the station numbers in the public repository.

We have included a sentence in Section 2.2 to explain the enumeration: "CTD station numbers follow the original enumeration used during NBP17-04, so they are more easily traceable to the hydrographic data, which is archived as described below in the Data Availability section."

Comment 3: Please consider the number of significant figures used in estimated values throughout the paper. For example in Tables 1 & 2 estimates are given to 4 significant figures and 2 decimal places which greatly exceeds the uncertainty in the estimate.
Thank you, we have corrected the number of significant figures used throughout the tables.

Comment 4: I very much appreciated the detailed laying out of calculations in the Supplementary material. However, while I followed Supplemental 1, I could not understand the derivation of Concsalt in Supplemental 2 and 3. I do not understand why you use ice

the quotient of the integrals (S3.3) to represent the integral of the quotient (i.e. the integral of (S3.2)). Please could you clarify.

Thank you for catching the error on our derivation of the frazil mass from the salinity anomaly. We agree with your assessment that we had applied the integral incorrectly when going from Step S3.2 to Step S3.3. Supplemental 3 has been changed to correct the formula. All calculations were redone and code was double checked.

The correction led to minor changes in the mass of ice and the concentration of ice, but those changes in the bulk inventories were not large enough to alter our interpretations.

Technical Corrections

line 36: I'm not sure what is meant by "one to two orders of magnitude better insulated"? Does it mean that the heat flux to the atmosphere is one to two orders of magnitude lower?

Thank you, edited for clarity.

Line 54: "eutectic freezing point" ? None of the cited works use the word "eutectic". I don't know if this is strictly incorrect but I did find it confusing since the "eutectic temperature" for sea ice is about −36oC (Vancoppenolle et al., 2019)

Vancoppenolle, M., Madec, G., Thomas, M., & McDougall, T. J. (2019). Thermodynamics of sea ice phase composition revisited. Journal of Geophysical Re- search:Oceans,124, 615–634. https://doi.org/10.1029/2018JC014611

Thank you, edited for clarity and removed.

Line 54: "Dmitrenko"

Thank you, corrected.

Lines 57-58: These are observed sizes so why not cite observations. Heorton & Feltham, 2017 and Wilchinsky et al., 2015 are modeling studies. Note Wilchinsky rather than Wlichinsky.

Thank you, corrected.

Line 62: incomplete sentence.

Thank you, corrected.

Line 64: Heorton & Feltham, 2017 and Wilchinsky et al., 2015 would fit well here. Additional relevant observational study that may be of use.

Ito, M., Ohshima, K., Fukamachi, Y., Simizu, D., Iwamoto, K., Matsumura, Y., . . . Eicken, H. (2015). Observations of supercooled water and frazil ice formation in an Arc- tic coastal polynya from moorings and satellite imagery. Annals of Glaciology, 56(69), 307-314. doi:10.3189/2015AoG69A839

Thank you, corrected and added.

Line 66: Suggest reference for statement re dense water formation; such as Oshima et al 2016.

Ohshima, K.I., Nihashi, S. & Iwamoto, K. Global view of sea-ice production in polynyas and its linkage to dense/bottom water formation. Geosci. Lett. 3, 13 (2016) doi:10.1186/s40562-016-0045-4

Thank you, corrected and added.

Lines 96-98: Suggest also compare with satellite observations, e.g. Oshima et al, 2016.

We added this paper and a few other satellite observation papers.

We have heavily revised section 6.2 – the discussion of previous sea ice production estimates. That section includes this paragraph on remote sensing: "Overall, these ice production estimates from in-situ data are larger than the seasonal production estimates derived from remote sensing products. Drucker et al (2011) used the AMSR-E instrument to obtain a seasonal average of 12 cm day^{-1} for years 2003-2008. Oshima et al, (2016) estimated 6 cm day^{-1} of seasonal production for the years 2003-2011, and Nihashi and Ohshima (2015) determined 7 cm day^{-1} for years 2003-2010. Finally, Tamura et al (2016) found production rates that ranged from 7-13 cm day^{-1}, using both ECMWF and NCEP Reanalysis products for 1992-2013, reflecting a greater degree of consistency in successive estimates, likely because of consistency in the estimation methods. "

Thank you for pointing us to the paper. We have added the comparison to microwave sensing production rates.

Line 115: Typo Petrelli et a;., 2008
Thank you, corrected.
Line 151: What is the implication of being deployed from the starboard Baltic Room? More importantly what sort of issues arose because of sampling in supercooled wa- ters? The very recent paper of Robinson et al (2019) may be of interest.

Thank you. This was a great paper to review and has been added to our references. The paper outlines two potential sources of bias that are a concern for us that are explained in detail here and have been added to Section 3.2:

1. Self-heating where the thermistor reads warmer than the water because of the heat that remains in the housing, etc. We did keep the CTD rosette at room temp, so there is a risk of this.
2. Ice formation on surfaces in the conductivity cell. We don't see this as a risk because of (1) - the sensor was warm before it went over the side.
3. In the first draft, we examined and discussed the potential for frazil ice crystals passing thru the conductivity cell.

We think (2) did not take place because the cell was filled with saltwater prior to deployment. Freezing did take place at the beginning of the expedition, but this can be very damaging to a conductivity cell so steps were taken to avoid it.

Additionally, conductivity/salinity was increasing in our profiles. This is opposite the trend that Robinson et al (2019) observed. We address this question in more detail within section 3.2.

The protocol was to complete 2-3 minutes of soak time at around 10 m, until the spikes in the conductivity cell have completely gone away. We believe this dissipates much of the thermal

inertia, although a 10 minute soak time would have been better, the results suggest that 2-3 minutes will dissipate 70-80% of that excess heat in the sensor body.

While Robinson recommended using upcasts to avoid the thermal problem, this is complicated because the CTD sits at the bottom of the rosette, so the upcast can be influenced by turbulence and smoothing around the large 24 bottle, 2 ton rosette package.

Nevertheless, we examined upcasts and found that many of them were consistent with the results form the downcast – both for temperature and salinity. We have included a figure in the supplemental that highlights this.

The below figure was added as Supplemental Figure 1. For Station 25 you can see the salinity and temperature anomaly is reduced for the up cast which we attribute to the wake. For station 32, there is missing data in the up cast which would have impacted our calculations.

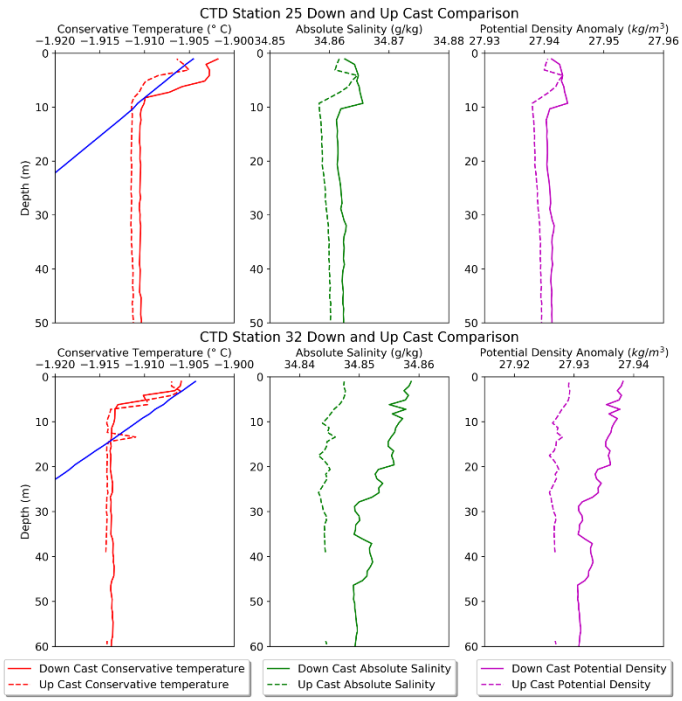

Lines 169-171: Care needs to be taken because the magnitude of the supercooling depends on the standard used. For example Nelson et al (2017) state "in situ super- cooling is larger (~ 0.003 K) when using TEOS-10 compared with EOS-80."
Nelson, M., Queste, B., Smith, I., Leonard, G., Webber, B., & Hughes, K. (2017). Measurements of Ice Shelf Water beneath the front of the Ross Ice Shelf using gliders. Annals of Glaciology, 58(74), 41-50. doi:10.1017/aog.2017.34
We have added a sentence in Section 2.3 stating that the choice of empirical relationship can affect the absolute freezing point calculation and we have included this citation, thank you for pointing this out.

Line 179: How were data normalized to 10 meters? I assume log boundary layer.
Thank you, correct we used a logarithmic wind profile.

Line 190: Suggest “near katabatic winds (> 10 ms−1) lasting”
Thank you, corrected.
Section 3.1: The reader would have more confidence in this section is the sampling protocol was detailed (see comment on line 151).
Thank you. We have added more details to our sampling procedures.
Line 220: “plots (a-k)”
Thank you , corrected.
Fig 4 & Fig 5: Again more description of the temperature of the instrument when it enters the water is needed in order to interpret these figures.
Lines 248 & 250: What was the uncertainty in determining the baseline for temperature and salinity?
Line 254: Consult Nelson et al (2017) and Robinson et al (2019)

Please refer to our related responses above and in the revised manuscript.

We have revised Section 2.3 to be more descriptive with the CTD sampling procedure.

Line 258: Incorrect citation. Should be (Skogeth et al, 2009)
Thank you, corrected.

Lines 265-268: Check procedures with respect to Robinson et al (2019)
We did not find any reference to or guidance on averaging procedures Robinson et al (2020). As discussed, we investigated the effect of averaging over different vertical intervals and found no systematic influence.

Line 293 & 302: remove hyphen in “super-cooling” for consistency as used “supercool- ing” in other places.
Thank you, corrected
Line 296: “0.5 to 1 ‰ ” NOT “0.5 to 1 % ”. This may mean that the statement on lines 303-305 needs to be reconsidered.
Thank you, corrected. I updated it to use g kg-1 to be consistent throughout the paper.
Line 298-299: Consider the number of decimal places in relation to the error in the measurement.
Thank you both reduced to the appropriate number of significant figures.
Section 3.5: I’m not sure if this section is necessary.
Thank you eliminated in favor of shortening the article.
Line 311: “Ice Shelf Water” is not defined. Also later in paper ISW is used and this also needs to be defined.
Thank you, defined. Section Removed.
Line 312: “(Rees Jones & Wells, 2018)” NOT “(Jones & Wells, 2018)”

Thank you. Section Removed.

Lines 313 & 315: “Robinson et al (2014)” NOT “Robinson et al (2017)”
Thank you. Section Removed.

Line 340: Remove “?”
Thank you corrected.
Line 342: “and movement”? of pack ice
Thank you, sentence removed in favor of shortening the article.
Line 363-364 and 398-399: What is the “starting location”? Why 10 m? Why does 10 m eliminate selection bias? Please consider rewriting.
Thank you, reworded. The variance in the temperature and salinity was less than the order the precision of the instrument. We cited the precision in Section
Equation (2): Is Conctemp the same as ConcT in Table 1? Please be consistent with ice ice notation.
Thank you corrected.
Line 381: lower case “w”
Thank you corrected.

Line 393: “Supplementals 2 and 3”
Thank you corrected.

Line 400: This is an example of Comment 1 above.
Thank you corrected.
Equations (3) and (4): What is H? Is this zS in the Suppplemental?
Thank you corrected to reflect the integral from the surface to zS. H was removed for clarity and consistency.
Equation (5): Concsalt the same as ConcS in Table 2? Please be consistent with Ice ice notation.
Thank you corrected.
Lines 424-426: Surely you could argue that the humidity was high because of evapo- ration.
Thank you edited for clarity.
Table 1: Please see Comment 3.
Line 477: “Robinson et al (2014)” NOT “Robinson et al (2017)”
Thank you corrected.
Line 479: ISW is not defined
Thank you corrected and defined.
Lines 486-487: I understood that the smallest eddies controlled the rate of dissipation. However the arguments of the energy cascade equate the rate at which energy was injected at the largest scales to the rate of energy dissipation at the smallest scales (e.g. see Fig 8.3 Cushman-Roisin, 2019). This I agree with equation (6).
Thank you. Clarified and corrected.

Line 488: “Cushman-Roisin, 2019” NOT “Cushman-Rosin, 2019”
Thank you corrected.
Line 490: Insert “TKE” after “turbulent kinetic energy”
Thank you corrected.
Equation (8) & (11): I find the use of * to mean × very confusing.

Thank you. It has been removed from all equations.
Line 518: what does roughness class 0 imply? It does seem very small.
Roughness class 0 implies a ocean or sea surface
Khalfa, Dalila & Abdelouahab, Benretem & Herous, Lazhar & Issam, Meghlaoui. (2014). Evaluation of the adequacy of the wind speed extrapolation laws for two different roughness meteorological sites. American Journal of Applied Sciences. 11570583. 570-583. 10.3844/ajassp.2014.570.583

Line 534: delete "."
Thank you corrected.
Lines 544, 555, 562, 563, 587: please italicize variables
Thank you corrected.

Line 551: How is an "active depth layer" defined?
Thank you, edited for clarification.
Line 562: insert space
Thank you corrected.
Line 573: replace "A log-linear fit" with "A linear fit on a log-log scale"
Thank you corrected.
Line 578: replace "A logarithmic linear fit" with "A linear fit on a log-log scale"
Thank you corrected.
Lines 616-617: See Comment 3. I suggest rounding to 69, 28 and 10.

Line 621: "This other variations. . ."??
We have revised the wording.

Line 624: Insert "CI" after "confidence interval".
Thank you corrected.

Line 628: Delete" bin averaging"
Thank you corrected.

Table 2: Please see Comment 3.
Table 2, column TKE diss: Why to the power "-05"? Why not just "-5"?
Thank you corrected.
Table 2: Insert a note "MLD= mixed layer depth" – if it does??
It does, Thank you added.

Line 643: See Comment 3. I suggest rounding to 26.
Section 6.2: Note that from satellite studies Oshima et al (2016) quote an ice production rate of 8.4 m yr−1 (from Mar-Oct) which is about 35 cm day−1. This is close to your result.
Fig 10: This is a very interesting figure - I found it difficult to see and read the colors on top of the bathymetry color bar. I was not sure why bathymetry was needed. I wondered why it was so deep on the southern side of the Drygalski Ice Tongue? A simpler figure, an intuitive numbering of stations, and rounding of data would all make this figure have a higher impact in my opinion.

Thank you the figure was modified to make it easier to read the sea ice production rates.

We have revised this section (6.2) significantly to discuss the ice production rates.

Line 721: Roisin
Thank you corrected.

Line 784: D.W. Rees Jones
Thank you, reference removed since the context was removed.
Line 792: Ross Sea Thank you corrected.

Line 809: Arctic Thank you corrected.

Supplementals: Please see Comments 1, 3, and 4.
I think Equation (S1.5) is meant to be in Conctemp ice Thank you corrected.

Personal dislike of use of * to mean × "times" in Supplemental 2 and 3. Thank you, all removed.
What is x in Table S3? I assume that × "times" is meant. Yes, italics removed and spaces added.
Thank you

Review 2 Comments and Responses: Comments are in black and responses are in red

General comments

This study has revealed extremely high ice production via underwater frazil ice formation and the importance of intense events of frazil ice production in the Antarctic polynyas, based on direct observation under PIPERS project. The finding is novel and the method/analysis are appropriate. The study demonstrates that process of under- water frazil ice formation should be properly considered in the polynya process. In addition, observed polynyas are the sites where dense water, precursor of Antarctic Bottom Water, is formed. Therefore, I have no doubt that the contents of the paper contribute to understanding of sea ice –ocean interaction and the Antarctic oceanography significantly. Therefore, I highly recommend that the paper should be published in "Cryosphere", but with moderate revision. The revising points are listed below.

Major comments

1. This study estimated ice production for each event and shows large variance of ice production ranging from 7 to 378 cm day-1. Although these estimates are very valuable, an important quantity is the averaged ice production or annual (monthly) ice production, which controls the formation of dense water and thus Antarctic Bottom Water. Therefore, it is desirable to infer the averaged ice production based on the two-weeks' PIPERS project. The authors took the median value of 26 cm day-1 as a representative ice production. This is better than taking the average of all the events, considering the very large variance. Even so, the median seems somewhat ad hoc way. More reasonable estimate of representative or average ice production may be possible. For example, if ice production can be related to atmospheric (and oceanic) conditions, more reasonable estimate of average ice production would be possible. Once average or monthly ice production can be inferred, then comparison or discussion with the previous satellite estimates would be possible. The present study probably suggests that the previous satellite estimation underestimated the polynya ice production.

Thank you for the comment. We found that the production rate varied with respect to the wind and with respect to the location in the polynya. There was a direct relationship between wind speed and production rate. There was an inverse relationship between the distance from the coastline and the production rate.

We have taken careful consideration to produce the requested up-scaling to a seasonal average. This includes neglecting Station 35 as an outlier, because of possible ice shelf influence (See Section 6.0 for discussion). We have added a new section to the discussion, titled " 6.1 Seasonal Ice Production", which describes the method for up-scaling. Additional detail on the computation of the seasonal average can be found in Supplemental 7 and Supplemental Figure 6.

The results yielded a seasonal ice production of 29 cm day^{-1}.

2. Ice production has very large variance from 7 to 378 cm day-1. What are the key points (reasons) for this large variance? Brief statement for this is needed, because this seems very important part of this paper. Associated with this, as shown in Table 2, the life time is very short in the case of Stn.32. This is because Lm-o is very small. As such, the value of Lm-o has very large variance. What is the key factor for this?

The large variance is due in part to varying wind conditions and varied geographic position. The large difference at station 32 is due to a difference in the turbulent kinetic energy dissipation rate. It varies from the other stations by one order of magnitude. Station 32 experiences the most wind stress and a different SWIFT deployment was used to derive the TKE dissipation.
For station 35, the LMO is very small. That is due to a higher salt flux at that station and slower wind speeds. Station 35 represented the highest salt flux and the second smallest wind speed/stress. When the LMO is small mixing is buoyancy dominated, as opposed to wind shear dominated. We feel that the buoyancy is likely dominant due to ISW contributions.

Minor comments
3. Description in the paper is overall understandable. On the other hand, it is somewhat redundant and lacking in compactness. I think that the length of the paper can be reduced by 10-20%.
4. Line 362-363: Please describe the temperature trend and the starting location more specifically. Not easy to understand at this stage.
Thank you clarified.
5. Line 378-379: Lf=330 kJ kg-1: What is the reference for this value? I think that use of Lf=334 kJ kg-1 is more appropriate by referring Martin (1981), which showed that frazil ice crystals do not retain any brine and thus Lf should be equal to that of freshwater. Although 330 and 334 is not so different, the basis of the value should be described in the scientific paper.
Thank you corrected.
6. Line 380: Equation (2); Table 1: Conceˆtemp_ice is not understandable quantity. The total volume of frazil ice can be calculated by integration over the water column and this value can be represented by thickness of ice. This quantity is easier to under- stand. Heat loss occurs at the ocean surface, and thus a quantity per unit area is more meaningful than a quantity per unit volume. I know that ice production represented by thickness per day is introduced using Conceˆtemp_ice later in section 6. But integrated frazil ice thickness should be introduced at this stage. This comment is also applied to Conceˆsalt_ice (Equation 5).

We had an error in our calculation for the column integral of ice production. This has changed our estimate of the total column integrals by about 10%. One of the authors felt that the standard and most intuitive way to present frazil ice inventories is to present them as a concentration in kg/m^3. We have followed this protocol, and the calculation of ice concentration is defined in section 4.1. Arguably, few people have intuition for frazil amounts, but the representation as concentration can be related to other quantities.

7. Line 398: How did you determine the starting location from below the anomaly?

There were a small number of profiles, so this procedure was done graphically, using the profiles as they are shown in Figure 7. We have revised Section 4.1 to clarify the approach.

"Because we lacked multiple profiles at the same location, we were not able to observe the time evolution of these anomalies. Consequently, T_b represents our best inference of the temperature of the water column prior to the onset of ice formation; it is highlighted in Figure 7a with the dashed line. We established the value of T_b by averaging the temperature over a 10 m interval directly beneath the anomaly. In most cases, this interval was nearly isothermal and isohaline, as would be expected within a well-mixed layer. The uncertainty in the value of T_b was estimated from the standard deviation within this 10 m interval; the average was 7.5×10^{-5} °C, which is 1% of the temperature."

8. Line 417: Remove one of the double heat.
Thank you corrected.
9. Line 489: How "t" is finally represented using the known quantities?
Thank you, added from supplemental to main text.
10. Table 2: How "the life time" is finally represented (by an equation)?
Thank you, added.
11. Figure 10: color at Stn.32 looks like purple, not red.
Thank you figure updated.
12. Regarding the estimate of average or annual (monthly) ice production, there have been several satellite (microwave) investigations for these polynyas (e.g., Comiso et al., 2011; Drucker et al., 2011; Nihashi and Ohshima, 2015; Tamura et al., 2016), because the satellite microwave can provide daily sea ice condition. For example, data set of monthly ice production from Nihashi and Ohshima (2015) is now in public, and can be downloaded from http://www.lowtem.hokudai.ac.jp/wwwod/polar-seaflux/. As well as comparison with the model studies as was done in section 6.2, comparison and discussion with these satellite studies would enhance the value of this paper.

Thank you for pointing out these additional resources. We have included these references in the manuscriptWe have revised section 6.2 – the discussion of previous sea ice production estimates. That section includes this paragraph on remote sensing: "Overall, these ice production estimates from in-situ data are larger than the seasonal production estimates derived from remote sensing products. Drucker et al (2011) used the AMSR-E instrument to obtain a seasonal average of 12 cm day^{-1} for years 2003-2008. Oshima et al, (2016) estimated 6 cm day^{-1} of seasonal production for the years 2003-2011, and Nihashi and Ohshima (2015) determined 7 cm day^{-1} for years 2003-2010. Finally, Tamura et al (2016) found production rates that ranged from 7-13 cm day^{-1}, using both ECMWF and NCEP Reanalysis products for 1992-2013, reflecting a greater degree of consistency in successive estimates, likely because of consistency in the estimation methods. "

References
Comiso, J. C., R. Kwok, S. Martin, and A. L. Gordon, 2011: Variability and trends in sea ice extent and ice production in the Ross Sea. J. Geophys. Res., 116, C04021, doi:10.1029/2010JC006391.

Drucker, R., S. Martin, and R. Kwok, 2011: Sea ice production and export from coastal polynyas in the Weddell and Ross Seas. Geophys. Res. Lett., 38, L17502, doi:10.1029/2011GL048668.
Nihashi, S. and K.I. Ohshima, 2015: Circumpolar mapping of Antarctic coastal polynyas and landfast sea ice: relationship and variability. Journal of Climate, 28, 3650-3670, doi:10.1175/JCLI-D-14-00369.
Tamura, T., K. I. Ohshima, A. D. Fraser and G. D. Williams, 2016: Sea ice production variability in Antarctic coastal polynyas. Journal of Geophysical Research, 121, 2967- 2979, doi:10.1002/2015JC011537.

Frazil ice growth and production during katabatic wind events in the Ross Sea, Antarctica

Lisa De Pace[1], Madison Smith[2], Jim Thomson[2], Sharon Stammerjohn[3], Steve Ackley[4], and Brice Loose[5]

[1]Department of Science, US Coast Guard Academy, New London CT
[2]Applied Physics Laboratory, University of Washington, Seattle WA
[3]Institute for Arctic and Alpine Research, University of Colorado at Boulder, Boulder CO
[4]University of Texas at San Antonio, San Antonio TX
[5]Graduate School of Oceanography, University of Rhode Island, Narragansett RI

Correspondence to: Brice Loose (bloose@uri.edu)

ABSTRACT: During katabatic wind events in the Terra Nova Bay and Ross Sea polynyas, wind speeds exceeded 20 m s^{-1}, air temperatures were below -25 °C, and the mixed layer extended as deep as 600 meters. Yet, upper ocean temperature and salinity profiles were not perfectly homogeneous, as would be expected with vigorous convective heat loss. Instead, the profiles revealed bulges of warm and salty water directly beneath the ocean surface and extending downwards tens of meters. Considering both the colder air above and colder water below, we suggest the increase in temperature and salinity reflects latent heat and salt release during unconsolidated frazil ice production within the upper water column. We use a simplified salt budget to analyze these anomalies to estimate in-situ frazil ice concentration between 266 x 10^{-3} and 13 x 10^{-3} kg m^{-3}. Contemporaneous estimates of vertical mixing by turbulent kinetic energy dissipation reveal rapid convection in these unstable density profiles, and mixing lifetimes from 2 to 12 minutes. The corresponding median rate of ice production is 28 cm day^{-1} and compares well with previous empirical and model estimates. Our individual estimates of ice production up to 302 cm day^{-1} reveal the intensity of short-term ice production events during the windiest episodes of our occupation of Terra Nova Bay Polynya.

Formatted: Don't suppress line numbers

Deleted: 332

Deleted: 24.4

Deleted: 6

Deleted: 78

1. INTRODUCTION

Latent heat polynyas form in areas where prevailing winds or oceanic currents create divergence in the ice cover, leading to openings either surrounded by extensive pack ice or bounded by land on one side and pack ice on the other (coastal polynyas) (Armstrong, 1972; Park et al, 2018). The open water of polynyas is critical for air-sea heat exchange, since ice covered waters are better insulated and reduce the amount of heat flux to the atmosphere (Fusco et al., 2009; Talley et al, 2011). A key feature of coastal or latent heat polynyas are katabatic winds (Figure 1), which originate as cold, dense air masses that form over the continental ice sheets of Antarctica. These air masses flow as sinking gravity currents, descending off the glaciated continent, or in the case of the Terra Nova Bay Polynya, through the Transantarctic mountain range. These flows are often funneled and strengthened by mountain-valley topography. The katabatic winds create and maintain latent heat polynyas. This research focuses on in-situ measurements taken from two coastal latent heat polynyas in the Ross Sea, the Terra Nova Bay polynya and the Ross Sea polynya.

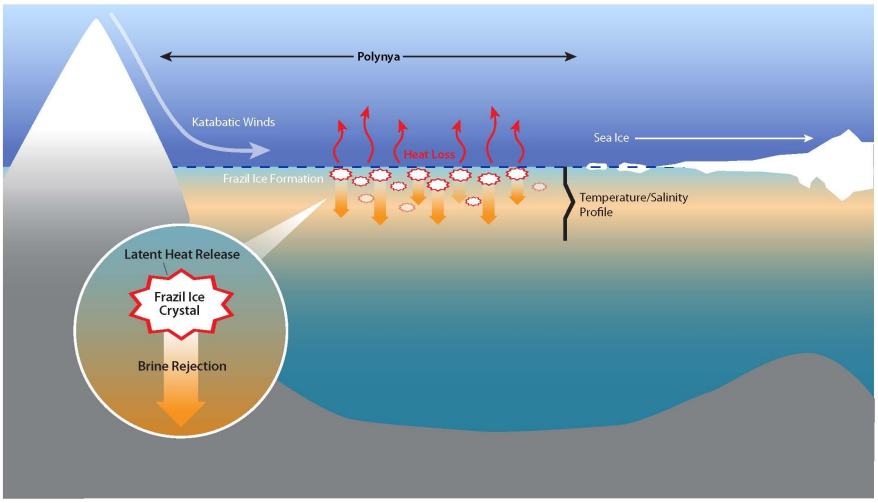

Deleted: one to two orders of magnitude

Figure 1: Schematic of a latent heat or coastal polynya. The polynya is kept open from katabatic winds which drive ice advection, oceanic heat loss and frazil ice formation. Ice formation results in oceanic loss of latent heat to the atmosphere and brine rejection. Inset is a schematic of Frazil ice formation that depicts the release of latent heat of fusion and brine rejection as a frazil ice crystal is formed.

The extreme oceanic heat loss in polynyas can generate supercooled water, which is colder than the freezing point (Skogseth et al., 2009; Dmitrenko et al, 2010; Matsumura & Ohshima, 2015), and is the precursor to ice nucleation. In turbulent, supercooled water sea ice formation begins with fine disc-shaped or dendritic crystals called frazil ice. These frazil ice crystals (Figure 1 inset) are about 1 to 4 mm in diameter and 1-100 μm thick (Martin, 1981). In polynyas, the frazil ice is transported downwind from the formation site and can mix over a region of 5-15 meters depth (Heorton et al, 2017; Ito et al, 2015). Katabatic winds sustain the polynya by clearing frazil ice, forming pancake ice which piles up at the polynya edge to form a consolidated ice cover (Morales Maqueda et al, 2004; Ushio and Wakatsuchi, 1993, Wilchinsky et al, 2015).

Brine rejection (Cox & Weeks, 1983) during ice production, can lead to dense water formation (Ohshima et al, 2016). Over the Antarctic continental shelf, this process produces a water mass known as High Salinity Shelf Water (HSSW) (Talley et al, 2011). In the case of the Ross Sea, the cold, dense HSSW formed on the shelf eventually becomes AABW off the shelf, the densest water in the abyssal ocean (Cosimo & Gordon, 1998; Jacobs, 2004; Martin, et al., 2007; Tamura et al.; 2007). Terra Nova Bay polynya produces especially dense HSSW, and produces approximately 1-1.5 Sv of HSSW annually (Buffoni et al., 2002; Orsi & Wiederwohl, 2009; Sansivero et al, 2017; Van Woert 1999a,b).

Given the importance of AABW to meridional overturning circulation, polynya ice production rates have been intensively studied. Gallee (1997), Petrelli et al. (2008), Fusco et al. (2002), and Sansivero et al. (2017) used models to calculate polynya ice production rates on the order of tens of centimeters per day. Schick (2018) and Kurtz and Bromwich (1985) used heat fluxes to estimate polynya ice production rates, also on the order of tens of centimeters per day. Drucker et al (2011), Ohshima et al (2016) Nihasi and Oshima (2015), and Tamura et al (2016) used satellite remote sensing using microwave sensors to estimate annual production rates on the

Deleted: (Talley et al, 2011)

Deleted: “

Deleted: ”

Deleted: eutectic

Deleted: . Supercooled water is

Deleted: and in-situ ice production

Deleted: The

Deleted: first type of

Deleted: to appear are found as

Deleted: millimeters

Deleted: micrometers

Deleted: in thickness

Deleted: Heorton & Feltham, 2017;

Deleted: ; Ushio & Wakatsuchi, 1993; Wlichinsky et al., 2015)

Deleted: .

Deleted: large net heat losses from katabatic winds and cold air temperatures eventually lead to frazil ice production. T

Deleted: crystals are

Deleted: where katabatic winds and cold air temperatures transport of ice crystals away from the formation site near the ocean surface and into the water column. Both conditions are achieved in polynyas by (Coachman, 1966). Katabatic winds

Deleted: away

Deleted: near the ocean surface

Deleted: and

Deleted: ed

Deleted: into the water column

Deleted: s

Deleted: (

Deleted: and latent heat release d

Deleted: .

Deleted: the precursor to Antarctic Bottom Water (AABW),

Deleted: global circulation

Deleted: global thermohaline circulation

Deleted: widely

Deleted: , and modeled, and measured via satellite oceanography

order of tens of kilometers cubed per year. However, the heterogeneous and disaggregated process of ice formation, that occurs on scales of um, and accumulates over km, in very harsh observational conditions makes it difficult to direct measurements that can lead to better mechanistic predictions (Fusco et al., 2009; Tamura et al., 2007).

1.2 Motivation for this article

Late autumn CTD profiles from the Ross Sea coastal polynyas revealed anomalous bulges of warmer, saltier water near the ocean surface during katabatic wind events. During these events, we observed wind rows of frazil ice aggregation. We hypothesized that the excess temperature was evidence of latent heat of release during frazil ice formation, and that the excess salinity was evidence of brine rejection from the same. We attempt to validate and confirm these observations by comparing the shape and size of the profile anomalies with estimates of the CTD precision and stability, and by using supporting evidence of the atmospheric conditions that are thought to drive frazil ice formation (e.g. temperature and wind speed). This analysis is described below, followed by our estimates of frazil ice concentration using the temperature and salinity anomalies (§4). To better understand the importance of frazil formation, we computed the lifetime of these anomalies (§5), which in turn yielded frazil ice production rates (§6). Last, we discuss the implications for spatial variability of ice production and application for further polynya sea ice production estimates.

2. STUDY AREA AND DATA

2.1 The Terra Nova Bay Polynya and Ross Sea Polynya

The Ross Sea, a southern extension of the Pacific Ocean, abuts Antarctica along the Transantarctic Mountains and has three recurring latent heat polynyas: Ross Sea polynya (RSP), Terra Nova Bay polynya (TNBP), and McMurdo Sound polynya (MSP) (Martin et al., 2007). The RSP is Antarctica's largest recurring polynya, the average area of the RSP is 27,000 km^2 but can grow as large as 50,000 km^2, depending on environmental conditions (Morales Maqueda, et al., 2004; Park et al, 2018). It is located in the central and western Ross Sea to the east of Ross

Deleted: quantitative estimation of polynya ice production is challenging due to the difficulty of obtaining

Deleted: During a late

Deleted: oceanographic expedition to the Ross Sea as part of the PIPERS (Polynyas, Ice Production and seasonal Evolution in the Ross Sea) project we measured

Deleted: in the

Deleted: Despite air temperatures that were well below freezing and strong winds frequently in excess of the katabatic threshold, these CTD profiles presented signatures of warmer water near the surface. The excess temperature was accompanied by similar signatures of saltier water. During this period

Deleted: , we also observed

Deleted: long

Deleted: fusion

Deleted: from

Deleted: frazil ice formation

Deleted: To test these hypotheses, w

Deleted: had to first evaluate the fidelity of these CTD

Deleted: measurements

Deleted:

Island, adjacent to the Ross Ice Shelf (Figure 2), and typically extends the entire length of the Ross Ice Shelf (Martin et al., 2007; Morales Maqueda et al., 2004). TNBP is bounded to the south by the Drygalski ice tongue, which serves to control the polynya maximum size (Petrelli et al., 2008). TNBP and MSP, the smallest of the three polynyas, are both located in the western Ross Sea (Figure 2). The area of TNBP, on average is 1300 km^2, but can extend up to 5000 km^2; the oscillation period of TNBP broadening and contracting is 15-20 days (Bromwich & Kurtz, 1984). This paper focuses primarily on TNBP and secondarily on RSP, where our observations were taken.

During the autumn and winter season, Morales Maqueda et al., (2004) estimated TNBP cumulative ice production to be around 40-60 meters of ice, or approximately 10% of the annual sea ice production that occurs on the Ross Sea continental shelf. The RSP has a lower daily ice production rate, but produces three to six times as much as TNBP annually due to its much larger size (Petrelli et al., 2008).

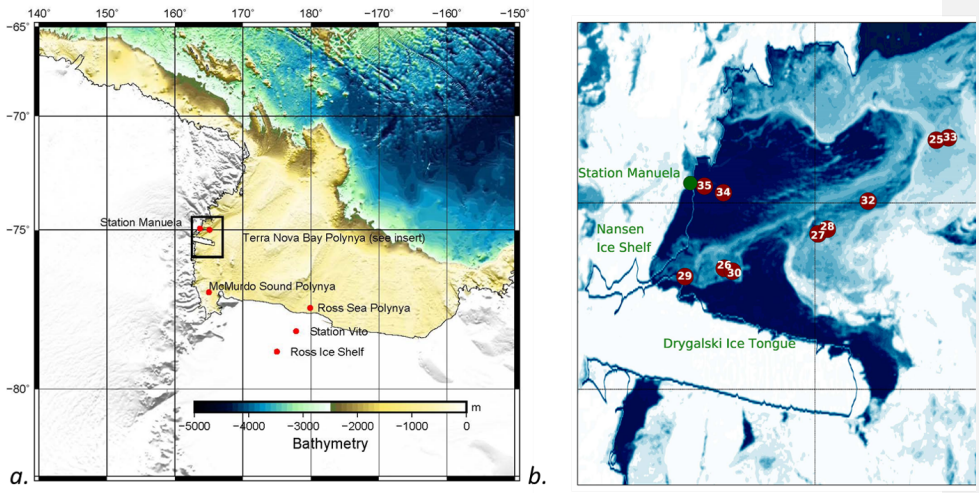

Figure 2: Map of the Ross Sea and the Terra Nova Bay Polynya. a) Overview of the Ross Sea, Antarctica highlighting the locations of the three recurring polynyas: Ross Sea Polynya (RSP), Terra Nova Bay Polynya (TNBP), and McMurdo Sound Polynya (MSP). Bathymetry source: GEBCO 1-degree grid. b) Terra Nova Bay Polynya Insert as indicated by black box in panel a.

MODIS image of TNBP with the 10 CTD stations with anomalies shown. Not included is CTD Station 40, the one station with an anomaly located in the RSP. (CTD Station 40 is represented on Figure 2a as the location of the Ross Sea Polynya.) Date of MODIS image is March 13, 2017; MODIS from during cruise dates could not be used due to the lack of daylight and high cloud clover.

2.2 PIPERS Expedition

We collected these data during late autumn, from April 11 to June 14, 2017 aboard the RVIB Nathaniel B. Palmer (NB Palmer, NBP17-04). More information about the research activities during the PIPERS expedition is available at http://www.utsa.edu/signl/pipers/index.html. Vertical profiles of Conductivity, Temperature, and Depth (CTD) were taken at 58 stations within the Ross Sea. For the purposes of this study, we focus on the 13 stations (CTD 23-35) that occurred within the TNBP and 4 stations (CTD 37-40) within the RSP during katabatic wind events (Figure 2). In total, 11 of these 17 polynya stations will be selected for use in our analysis, as described in §3.1.

2.3 CTD measurements

The CTD profiles were carried out using a Seabird 911 CTD (SBE 911) attached to a 24 bottle CTD rosette, which is supported and maintained by the Antarctic Support Contract (ASC). Between CTD casts, the SBE911 was stored at room temperature to avoid freezing components. Before each cast, the CTD was soaked at approximately 10 meters for 3-6 minutes until the spikes in the conductivity readings ceased, suggesting the pump had purged all air bubbles from the conductivity cell. Each CTD cast contains both down and up cast profiles. In many instances, the upcast recorded a similar thermal and haline anomaly. However the 24 bottle CTD rosette package creates a large wake that disturbs the readings on the up cast leading to some profiles with missing data points and more smoothed profiles, so only the wake uncontaminated down cast profiles are used (Supplemental Figure 1 offers a comparison of the up vs down casts).

The instrument resolution is important for this study, because the anomalous profiles were identified by comparing the near surface CTD measurements with other values within the same profiles. The reported initial accuracy for the SBE 911 is ± 0.0003 S m^{-1}, ± 0.001 °C, and 0.015% of the full-scale range of pressure for conductivity, temperature, and depth respectively.

Deleted: ¶

Deleted: ¶

Deleted: For each CTD deployment

Deleted: taken

Deleted: from

Deleted: and

Deleted: at

Deleted: and

Deleted: was primed

Deleted: The SBE 911 was deployed from the starboard Baltic Room. …

Deleted: upcast

Deleted: that would have led to unnecessary interpolation

Deleted: n example

Deleted: profiles

Deleted:

Independent of the accuracy stated above, the SBE 911 can resolve differences in conductivity, temperature, and pressure on the order of 0.00004 S m^{-1}, 0.0002 °C and 0.001% of the full range, respectively (SeaBird Scientific, 2018). The SBE 911 samples at 24 Hz with an e-folding time response of 0.05 seconds for conductivity and temperature. The time response for pressure is 0.015 seconds.

The SBE 911 data were processed using post-cruise calibrations by Seabird, following standard protocol, and quality control parameters. Profiles were bin-averaged at two size intervals: one-meter depth bins and 0.1-meter depth bins, to compare whether bin averaging influenced the heat and salt budgets. We observed no systematic difference between the budget calculations derived from one-meter vs 0.1-meter bins; the results using one-meter bins are presented in this publication. All thermodynamic properties of seawater were evaluated via the Gibbs Seawater toolbox, which uses the International Thermodynamic Equation Of Seawater – 2010 (TEOS-10). It should be noted that the freezing point calculation can vary slightly, depending on the choice of empirical relationships that are used (e.g. TEOS-10 vs. EOS-80, Nelson et al., 2017).

2.4 Weather observations

Weather observations from the NB Palmer meteorological suite during these periods were compared with observations from automatic weather stations Manuela, on Inexpressible Island, and Station Vito, on the Ross Ice Shelf (Figure 2a). Observations from all three were normalized to a height of 10 meters using the logarithmic wind profile (Figure 3). The NB Palmer was in TNB from May 1 through May 13; during this period the hourly wind speed and air temperature data from Weather Station Manuela follow the same pattern, with shipboard observations from the NB Palmer observations being lower in intensity (lower wind speed, warmer temperatures) than Station Manuela. In contrast, the wind speed and air temperature from NB Palmer during its occupation in RSP (May 16-18) is compared to Station Vito. At Station Vito, the air temperature is colder, but the wind speed is less intense. Whereas at Station Manuela (TNBP) the winds are channelized and intensified through adjacent steep mountain valleys, the winds at Station Vito (RSP) are coming off the Ross Ice Shelf, resulting in lower wind speed.

Deleted: post-
Deleted: with
Deleted: Since we
Deleted: ,
Deleted:
Deleted:
Deleted: ¶
¶
Deleted: Multiple katabatic wind events were observed within the TNBP and RSP during the PIPERS expedition.

During the CTD sampling in the TNBP there were 4 periods of intense katabatic wind events, with each event lasting for at least 24 hours or longer. During the CTD sampling in the RSP there was just one event of near katabatic winds (> 10 ms^{-1}) lasting about 24 hours. During each wind event, the air temperature oscillated in a similar pattern and ranged from approximately -10 °C to -30 °C.

Formatted: Superscript

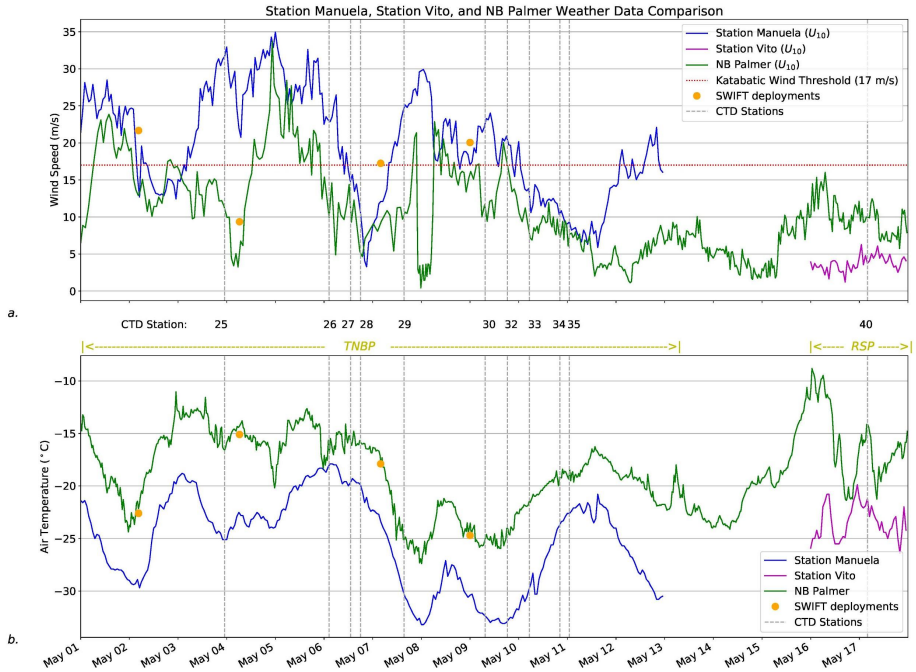

Figure 3: Weather observations from 01 May to 17 May 2017. a.) Wind speed from Station Manuela (blue line), Station Vito (purple line), NB Palmer (green line), and SWIFT (orange marker) deployments adjusted to 10 meters. The commonly used katabatic threshold of 17 m s^{-1} is depicted as a "dotted red line", as well as the date and start time of each CTD cast. b) Air temperature from Station Manuela, Station Vito, NB Palmer, and SWIFT deployments.

3. EVIDENCE OF FRAZIL ICE FORMATION

3.1 Selection of profiles

We used the following selection criteria to identify profiles from the two polynyas that appeared to show frazil ice formation: (1) a deep mixed layer extending several hundred meters (Supplemental Figure 2), (2) in-situ temperature readings below the freezing point in the near-surface water (upper five meters), and (3) an anomalous bolus of warm and/or salty water within the top twenty meters of the profile (Figure 4 and 5 plots). For context, all temperature profiles acquired during PIPERS (with the exception of one profile acquired well north of the Ross Sea continental shelf area at 60°S, 170°E) were plotted to show how polynya profiles compared to those outside of polynyas (Supplemental Figure 2).

Deleted: be influenced by

Deleted: 1

Deleted: 1

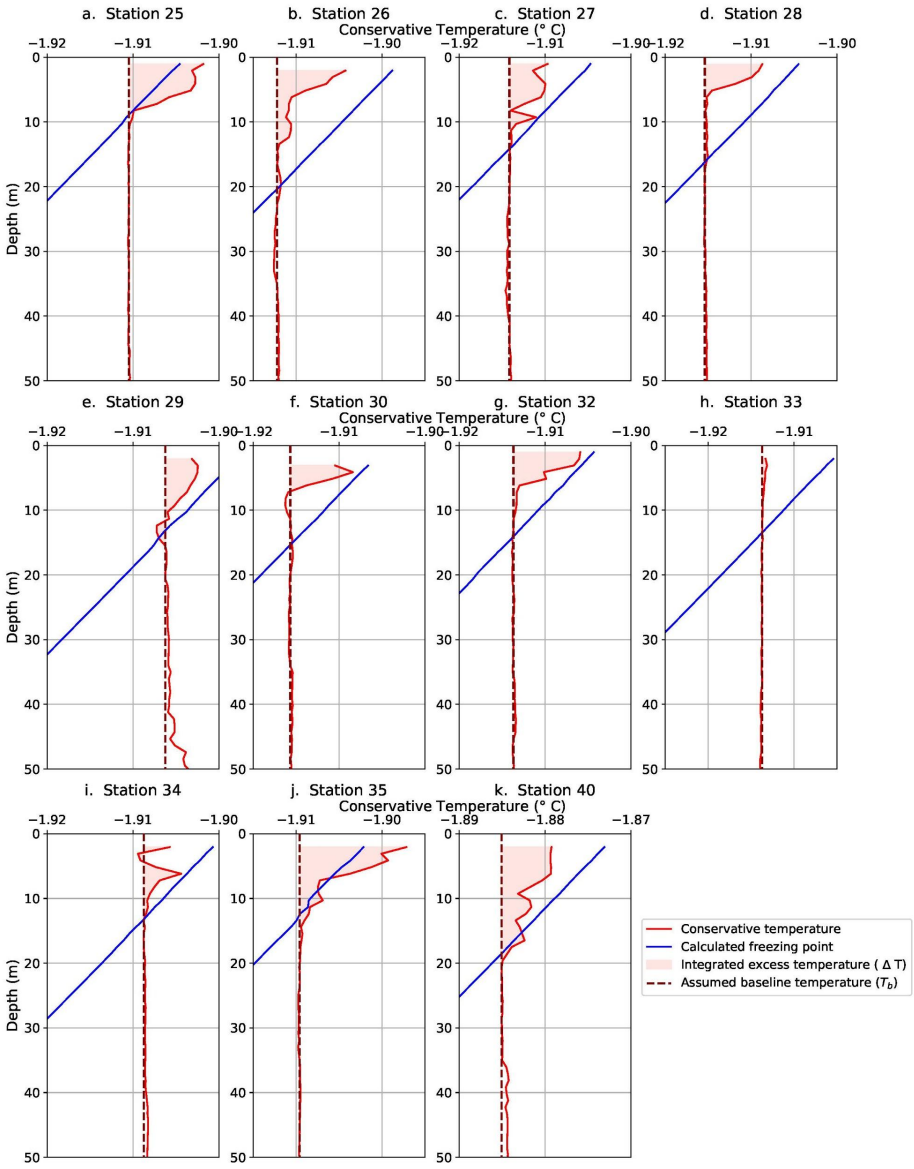

Figure 4: Conservative Temperature profiles from CTD down casts from 11 stations showing temperature and/or salinity anomalies. Plots (a-g) and (j-k) all show an anomalous temperature

Deleted: Profiles

bulge. They also show supercooled water at the surface with the exceptions of (a) and (j). All of the plots (a- k) have an x-axis representing a 0.02 °C change. Profiles (a-j) are from TNBP, and (k) is from RSP.

Deleted: h

Polynya temperature profiles were then evaluated over the top 50 meters of the water column using criteria 2 and 3. Nine TNBP profiles and one RSP profile exhibited the excess temperature anomalies over the top 10-20 m and near-surface temperatures close to the freezing point (Figure 4). Excess salinity anomalies (Figure 5) were observed at the same stations with two exceptions: Station 26 had a measurable temperature anomaly (Figure 4b) but no discernible salinity anomaly (Figure 5b), and Station 33 had a measurable salinity anomaly (Figure 5h) but no discernible temperature anomaly (Figure 4h). The stations of interest are listed in Table 1.

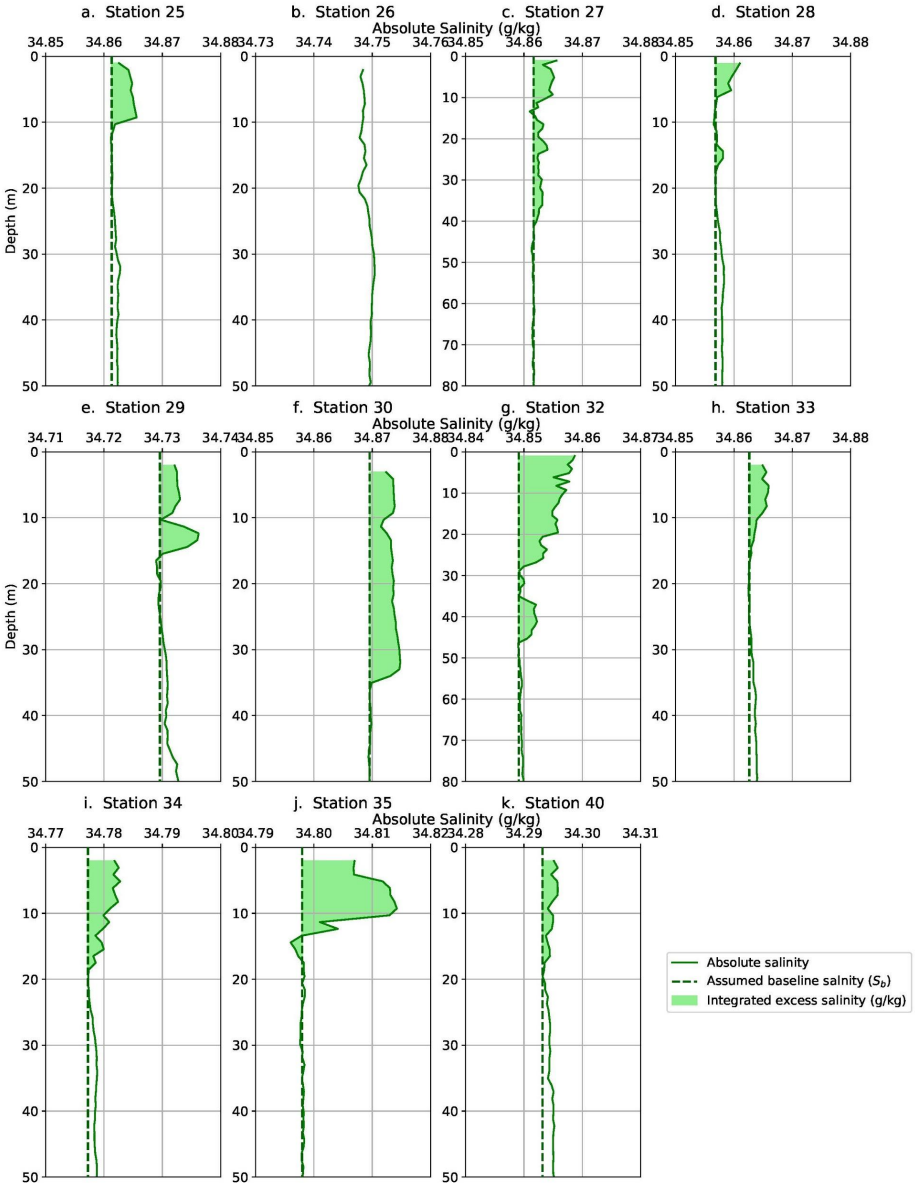
a. Station 25
b. Station 26
c. Station 27
d. Station 28
e. Station 29
f. Station 30
g. Station 32
h. Station 33
i. Station 34
j. Station 35
k. Station 40
Absolute Salinity (g/kg)
Depth (m)
Absolute salinity
Assumed baseline salnity (S_b)
Integrated excess salinity (g/kg)

339

Figure 5: Absolute Salinity profiles from CTD down casts from 11 stations showing temperature and/or salinity anomalies. Profiles (a) and (c-k) show an anomalous salinity bulge in the top 10-20 meters. Two profiles (c and g) show salinity anomalies extending below 40 meters, so the plot was extended down to 80 meters to best highlight those. All of the plots (a-k) have an absolute salinity range of 0.03 g kg^{-1}.

3.2 Evaluating the uncertainty in the temperature and salinity anomalies

We compared the magnitude of each thermal anomaly to the reported accuracy of the SBE 911 temperature and conductivity sensors: ± 0.001 °C and ± 0.0003 S m^{-1}, or ±0.00170 g kg^{-1} when converted to absolute salinity. To quantify the magnitude of the temperature anomaly, we computed a baseline excursion, $\Delta T = T_{obs} - T_b$, throughout the anomaly where T_{obs} is the in-situ conservative temperature and T_b is the in-situ baseline, which is extrapolated from the far field conservative temperature within the well-mixed layer below the anomaly (Figure 4). The largest baseline excursion from each of the 11 anomalous CTD profiles, averaged together, yields a value of ΔT = 0.0064 ◦C. While this is a small absolute change in temperature, it is still 32 times larger than the stated precision of the SBE 911 (0.0002 °C). The same approach was applied to the salinity anomalies yielded an average baseline excursion of 0.0041 S m^{-1} (or 0.0058 g kg^{-1} for absolute salinity), which is 100 times larger than the instrument precision (0.00004 S m^{-1}). Table 1 lists the maximum temperature and salinity anomalies for each CTD station.

The immersion of instruments into supercooled water can lead to a number of unintended outcomes as instrument surfaces may provide ice nucleation sites, or otherwise perturb an unstable equilibrium. Robinson et al., (2020) highlight a number of the potential pitfalls. One concern was that ingested frazil ice crystals could interfere with the conductivity sensor. Crystals smaller than 5 mm can enter the conductivity cell, creating spikes in the raw conductance data. Additionally, frazil crystals smaller than 100 µm would be small enough to pass between the conductivity electrodes and decrease the resistance/conductance that is reported by the instrument (Skogseth et al, 2009; Robinson et al, 2019). To test for ice crystal interference, the raw (unfiltered with no bin averaging) salinity profile was plotted using raw conductivity

Deleted: To evaluate the uncertainty associated with the temperature and salinity anomalies at each of the polynya stations, w
Deleted: initial
Deleted: maximum
Deleted: amount
Deleted: the baseline excursion
Deleted: ΔT, was calculated
Deleted: $\Delta T = T_{obs} - T_b$,
Deleted: Taking the single
Deleted: l
Deleted: and
Deleted: ing
Deleted: them
Deleted: we compute an average
Deleted: baseline excursion of
Deleted: the
Commented [BL1]: Isn't it Robinson 2020?
Formatted: Highlight
Formatted: Highlight
Moved down [2]: The sampling procedures followed do not strictly adhere to those outlined in Robinson et al (2019) introducing 3 potential sources of bias, self-heating where the thermistor reads warmer than the water due to the residual heat, ice formation on the conductive cell, and frazil crystals passing through the cell. Ice formation on the conductive cell is unlikely as the sensor was warm when it went into the water. Increased soak time would have helped to increase the thermal inertia but may not have eliminated it.
Deleted: It is conceivable that ice c
Deleted: be sucked into
Deleted:
Deleted: are
Deleted: theoretically
Deleted: float
Deleted: thereby
Deleted: & Smedsrud
Deleted: absolute

compared with the 1-meter binned data for the 11 anomalous CTD Stations (Supplemental Figure 3). The raw data showed varying levels of noise as well as some spikes or excursions to lower levels of conductance; these spikes may have been due to ice crystal interference. Overall, the bin-averaged profile does not appear to be biased or otherwise influenced by the spikes, which tend to fall symmetrically around a baseline. This was demonstrated by bin-averaging over different depth intervals as described in §2.4. It is also worth pointing out that the effect of these conductivity spikes would be to decrease the bin-averaged salinity, thereby working against the overall observation of a positive baseline excursion. In other words, the entrainment of frazil crystals could lead to an underestimate of the positive salinity anomaly, rather than the production of positive salinity aberration.

Another pitfall highlighted by Robinson et al., (2020) was the potential for self-heating of the thermistor by residual heat in the instrument housing. The results from their study reveal a thermal inertia that dissipates over a period of minutes. We examined the temperature trace during the CTD soak and did not observe this same behavior. It is possible that some thermal inertia did exist at the time of deployment, but any residual heat appeared to dissipate very quickly, compared to the 3-6 minute soak time before each profile. We suggest the self-heating might be a problem that arose in a single instrument, but is not necessarily diagnostic of all SBE 911 models. Those authors did not document this behavior in multiple instruments. Lastly, the potential for ice formation on the surface of the conductivity cell seems unlikely because it was kept warm until it was deployed in the water.

The observation of both warm and salty temperature anomalies cannot easily be explained by these documented instrument biases. A cold instrument might be subject to freezing in the conductivity cell, but this would not warm the thermistor that is physically separated from the cell. A warm instrument might have contained residual thermal inertia, which might have melted individual frazil ice crystals, but these would produce negative baseline excursions in salinity, rather than the positive anomaly. The anomalies we observed were found within 11 CTD stations, over the entire length of the polynya, and the same signature could be observed in the up and down cast, although the upcast was slightly smoothed.

Deleted: 2

Deleted: However

Deleted: data do

Deleted:

Deleted: ,

Deleted: Considering the consistency of the temperature and salinity measurements within and below the anomalies, and the repeated observation of

Deleted: at

Deleted: we infer that the observed anomalies are not an instrumental aberration.

Moved (insertion) [2]

Deleted: The sampling procedures followed do not strictly adhere to those outlined in Robinson et al (2019) introducing 3 potential sources of bias, self-heating where the thermistor reads warmer than the water due to the residual heat, ice formation on the conductive cell, and frazil crystals passing through the cell. Ice formation on the conductive cell is unlikely as the sensor was warm when it went into the water. Increased soak time would have helped to increase the thermal inertia but may not have eliminated it. ¶

3.3 Camera observations of frazil ice formation

During PIPERS an EISCam (Evaluative Imagery Support Camera, version 2) was operating in time lapse mode, recording photos of the ocean surface from the bridge of the ship every 10 minutes (for more information on the EISCam see Weissling et al, 2009). The images from the time in TNBP and RSP reveal long streaks and large aggregations of frazil ice. A selection of photos from TNBP were captured (Figure 6). The winds were strong enough at all times to advect frazil ice, creating downstream frazil streaks, and eventually pancake ice in most situations. Smaller frazil streaks and a curtain of frazil ice below the frazil streak were also visible.

Figure 6: Images from NB Palmer as EISCam (Evaluative Imagery Support Camera) version 2. White areas in the water are loosely consolidated frazil ice crystals being actively formed during a katabatic wind event. Image (d) was brightened to allow for better contrast.

3.4 Conditions for frazil ice formation

Deleted: ¶
Formatted: Indent: First line: 0"
Deleted: generate wave fields and
Deleted: thus
Deleted: ¶
¶
→
Deleted: during lab experiments

Laboratory experiments can provide a descriptive picture of the conditions that lead to frazil ice formation; these conditions are diagnostic of conditions in the TNBP. Ushio and Wakatsuchi (1993) exposed a 2 x 0.4 x 0.6 m tank tank to air temperatures of -10 °C and wind speeds of 6 m s^{-1}. They observed 0.1 to 0.2 °C of supercooling at the water surface and found that after 20 minutes the rate of supercooling slowed due to the release of latent heat, coinciding with visually observed frazil ice formation. After ten minutes of ice formation, they observed a measurable increase in temperature of the frazil ice layer of 0.07 °C warmer and 0.5 to 1.0 g kg^{-1} saltier, as a consequence of latent heat and salt release during freezing (Ushio and Wakatsuchi, 1993).

In this study, we found the frazil ice layer to be on average 0.006 °C warmer than the underlying water. Similarly, the salinity anomaly was on average 0.006 g kg^{-1} saltier than the water below. While the anomalies we observed were significantly smaller than those observed in the lab tank by Ushio and Wakatsuchi (1993), the trend of super-cooling, followed by frazil ice formation and the appearance of a salinity anomaly is analagous. The difference in anomalies can likely be explained by the reservoir size; the small volume of the lab tank will retain the salinity and temperature anomaly, rather than mixing it to deeper depths.

Considering the aggregate of supporting information, we infer that the anomalous profiles from TNBP and RSP were produced by frazil ice formation. The strong winds and sub-zero air temperatures (§2.4), reveal that conditions were sufficient for frazil formation, similar to the conditions observed in the laboratory. We showed that the CTD profiles in both temperature and salinity are reproducible and large enough to be distinguished from the instrument uncertainty (§3.1 and 3.2). Finally, the EISCam imagery reveals the accumulation of frazil ice crystals at the ocean surface.

4.0 ESTIMATION OF FRAZIL ICE CONCENTRATION USING CTD PROFILES

Having identified CTD profiles that trace frazil ice formation, we want to know how much frazil ice formation can be inferred from these T and S profiles. To estimate ice formation, the inventories of heat and salt from each profile can provide independent estimates of frazil ice concentration. To simplify the inventory computations, we neglect the horizontal advection of

Moved (insertion) [3]
Deleted: conducted laboratory experiments to reproduce the conditions observed in polynyas. They exposed their tank, [1]
Deleted: -m
Deleted: length,
Deleted: -m width and
Deleted: -
Deleted: depth to air temperatures at
Moved up [3]: conducted laboratory experiments to
Deleted: supercooling in the range of
Deleted: -c
Deleted: Simultaneously with the formation of frazil ice... [2]
Deleted: was
Deleted: the layer was
Deleted: %
Deleted: 4
Deleted: 58
Deleted: , which equates to 0.017% saltier
Deleted: our
Deleted: same
Deleted: was observed during PIPERS
Deleted: However, the forcing conditions and spatial ... [3]
Deleted: ¶
Deleted: ¶ ... [4]
Deleted: ¶ ... [5]
Deleted: Throughout Sections 2 and 3, we have documented ... [6]
Deleted:
Deleted: appear to
Deleted: trace
Deleted: In §2.4, t
Moved down [4]: supported both ice formation and
Deleted: §3.3 the coincident EISCam measurements
Deleted: reveal significant accumulation of frazil ice crystals ... [7]
Moved (insertion) [4]
Deleted: supported both ice formation and advection. In §3.4 ... [8]
Deleted: noise
Deleted: InIn §3.4 and §3.5, we note the commonalities ... [9]
Deleted: a collection of
Deleted: ?
Deleted: Can we attribute a large portion of polynya ice. [10]
Deleted: the inventories

heat and salt; this is akin to assuming that lateral variations are not important because the neighboring water parcels are also experiencing the same intense vertical gradients in heat and salt. We first describe the computation using temperature in § 4.1 and the computation using salinity in § 4.2.

4.1 Estimation of frazil ice concentration using temperature anomalies

Using the latent heat of fusion as a proxy for frazil ice production we estimated the amount of frazil ice that must be formed in order to create the observed temperature anomalies. We estimated the excess enthalpy using the same temperature baseline excursion; $\Delta T = T_{obs} - T_b$, defined in §3.2 . The excess over the baseline is graphically represented in Figure 7a. Because we lacked multiple profiles at the same location, we were not able to observe the time evolution of these anomalies. Consequently, T_b represents our best inference of the temperature of the water column prior to the onset of ice formation; it is highlighted in Figure 7a with the dashed line. We established the value of T_b by averaging the temperature over a 10 m interval directly beneath the anomaly. In most cases, this interval was nearly isothermal and isohaline, as would be expected within a well-mixed layer. The uncertainty in the value of T_b was estimated from the standard deviation within this 10 m interval; the average was XXXX.

Deleted: We used the temperature profiles to compute the "excess" heat inside the anomalies. Utilizing

Deleted: For each station, we first estimated the enthalpy inside the temperature anomaly (Talley et al, 2011) as follows. Within each CTD bin, we

Deleted: as

Deleted: where T_{obs} is the in-situ conservative temperature and T_b is the in-situ baseline or far field conservative temperature…

Formatted: Highlight

Formatted: Subscript, Highlight

Formatted: Highlight

Commented [BL2]: Lisa, did you estimate this? I think so.

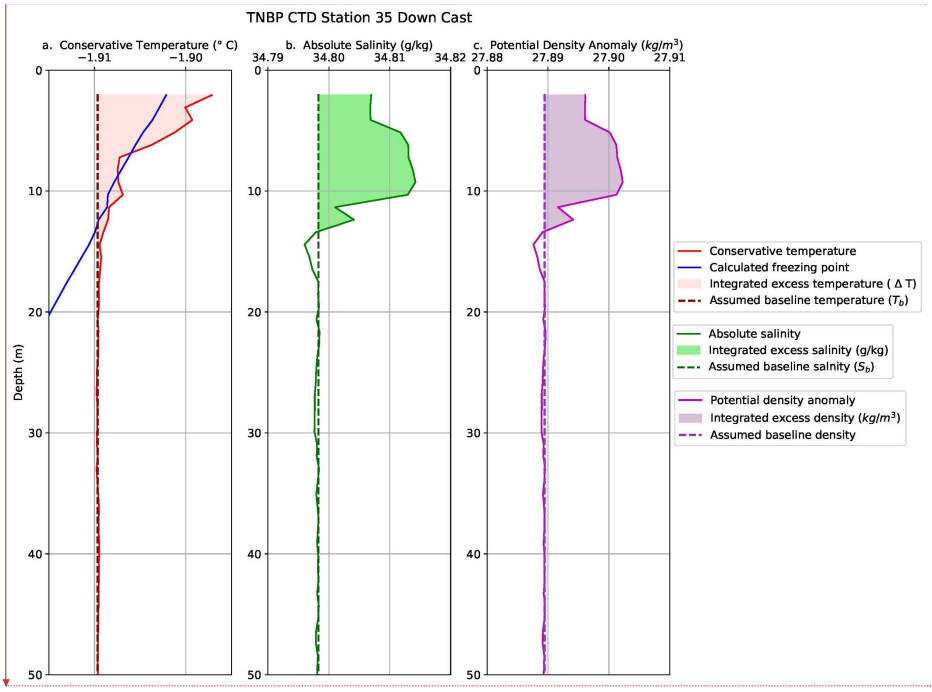

Figure 7: Conservative temperature, absolute salinity, and potential density anomaly for TNBP CTD Station 35, May 10, 2017. a) Conservative temperature profile showing the temperature anomaly, the selected baseline temperature (dashed line) and the integrated excess temperature (shaded area). b) Absolute salinity profile showing the salinity anomaly, the selected baseline salinity (dashed line), and integrated excess salinity (shaded area). c) Potential density anomaly showing the selected baseline density (dashed) and the excess density instability (shaded).

To find the excess heat (Q_{excess}^{total}) represented in the total thermal anomaly, we computed the vertical integral of heat per unit area from the surface (z=0) to the bottom of the anomaly (z=z_T):

$$Q_{excess}^{total} = \int_{z=0}^{z=z_T} \rho \; C_p \; \Delta T \; dz \qquad (1)$$

Here ρ is density of seawater, z is the depth range of the anomaly, and C_p is the specific heat capacity, The concentration of frazil ice is estimated by applying the latent heat of formation (L_f =330 kJ kg^{-1}) as a conversion factor to Q_{excess}^{total} :

Commented [BL3]: It is unfortunate that Station 35 has been called into question. I think maybe we should use another station to highlight in this figure. Maybe Station 32? I am open if you have another preference.

Deleted: looking for a near constant value of temperature in the profile directly below the temperature bulgeanomaly. In most cases the temperature trend was nearly linear, as one would expect of a mixed layer. and close to the freezing point. After selecting the starting locationOnce deeper than the anomaly and when the conservative temperature profile reached a near constant value, , the conservative temperature the conservative temperature was averaged over 10 meters (10 values from the 1-m binned data) to eliminate slight variations that in conservative temperature well beyond the precision of the SBE 911. ons and any selection bias. ¶

Deleted:

Deleted: =d

Deleted:

Deleted: =

Deleted: =

Commented [BL4]: 330 is correct for our T and S. Pat was not crected

Deleted: 4

Deleted: 0

$$Conc_{ice}^{temp} = \frac{Q_{excess}^{total}}{L_f \, z_T} \quad (2)$$

Where z_T is the depth of the temperature anomaly in meters. The concentration of ice derived represents the total concentration of ice, in kg m^{-3}. A more detailed explanation of equations 1 and 2 is contained in Supplemental 1. The mass concentration of ice derived from the temperature anomaly for each station is listed in Table 1.

4.2 Estimation of frazil ice concentration using salinity anomalies

The mass of salt within the salinity anomaly was also used to estimate ice formation. Assuming that frazil ice crystals do not retain any brine and assuming there is negligible evaporation, the salinity anomaly is directly proportional to the ice formed. By using the conservation equations for water and salt, the mass of frazil ice can be estimated by comparing the excess salt (measured as salinity) with the amount of salt initially present in the profile, similar to the inventory for heat. The complete derivation can be found in Supplemental 2. The salinity anomaly (ΔS) above the baseline salinity (S_b) is $\Delta S = S_{obs} - S_b$, and is shown in Figure 7b. The initial value of salinity (S_b) was established by observing the trend in the salinity profile directly below the haline bulge; in most cases the salinity trend was nearly linear beneath the bulge, however in general the salinity profiles were less homogeneous than the temperature profiles. We tried to select the starting location as where the anomaly ended and the expected mixed layer traits began. After selecting the starting location from below the anomaly, the absolute salinity was averaged over the next 10 meters to establish a baseline salinity.

To find the total mass of frazil ice ($Mass_{ice}^{S}$, kg m^{-2}) in the water column, the integral is taken the salt ratio times the mass of water ($M_W^O = \rho_b dz$, where ρ_b= assumed baseline density= 1028 kg m^{-3})). The concentration of ice ($Conc_{Ice}^{salt}$, kg m^{-3}) can be found by dividing the mass of frazil ice by the depth of the salinity anomaly (z_s). The resulting estimates of ice concentration are listed in Table 1.

$$Mass_{ice}^{S} = \rho_b \int_{z=0}^{z=z_S} \frac{\Delta S}{S_{obs}} dz \quad (3)$$

$$Conc_{ice}^{salt} = \frac{Mass_{Ice}^{S}}{z_S} \quad (4)$$

A more detailed explanation of equations 3 and 4 is contained in Supplementals 2 and 3.

Deleted: *

Deleted: ¶

Deleted: o

Deleted: of mass

Deleted: The conservation of mass equations used and subsequent …

Deleted: s

Deleted: are

Deleted: After

Deleted: integral of each component of the salt ratio is taken over the depth range of the anomaly

Deleted: This integral is multiplied by the total mass of water per area ($Mass_{Water}^{Total}$, kg m^{-2}) initially in the depth range of the anomaly.

Deleted: $Mass_{Water}^{Total} * \frac{\int_{z=0}^{z=H} \Delta S \, dz}{\int_{z=0}^{z=H} S_{obs} \, dz}$

Deleted: →→→→

Deleted: ¶

Commented [LDP5]: Correctedto reflect RC1- Comment 4. Given that we have the supplemental, I felt like i made sense to drop an equation.

Deleted: $Mass_{Water}^{Total} = \rho_b * \int_{z=0}^{z=H} dz$→→→→→→ →→(4)

Deleted: 5

Deleted: ,

Deleted: , and 5

4.3 Summary of the frazil ice estimates

The derived ice concentrations are listed in Table 1. The salt inventories yielded frazil ice concentrations from 13 x 10^{-3} kg m^{-3} to 266 x 10^{-3} kg m^{-3}. These estimates were 2 to 9 times larger than the estimates from the heat inventories. The difference is likely produced by heat loss to the atmosphere. Sensible and longwave heat exchanges produce an atmospheric loss term in the heat inventory, which has no corresponding influence on the salt inventory. Therefore, we suggest that derived ice concentrations from the heat anomalies underestimated frazil ice concentration in comparison to the salt inventory. We also note the salt inventory has neglected evaporation. Mathiot et al. (2012) found that evaporation had a small effect on salinity increases, when compared to ice production and contributed < 4% to salt flux. In the TNBP, the Palmer meteorological tower revealed high relative humidity (on average 78.3%), which indicates that there is likely some evaporation that would reduce the mass of ice derived from the salinity anomaly by small (<4%) margin.

Table 1: CTD Stations with temperature and salinity anomalies (See Figures 4-5), showing maximum values of the temperature anomaly, depth range of the temperature anomaly, concentration of ice derived from the temperature anomaly (§4.1), as well as the maximum value of the salinity anomaly, depth range of salinity anomaly, and concentration of ice derived from the salinity anomaly (§4.2).

Station	Date and Time	Maximum Δ T (°C)	z_T(m)	$Conc_{ice}^{temp}$ (kg m^{-3})	Maximum ΔS (g kg^{-1})	z_S(m)	$Conc_{ice}^{S}$ (kg m^{-3})
25	May 03 23:00:41	0.009	11.34	48 x 10^{-3}	0.004	13.4	67 x 10^{-3}
26*	May 06 02:30:08	0.008	24.73	14 x 10^{-3}	--	--	--
27	May 06 13:08:11	0.005	15.45	22 x 10^{-3}	0.003	41.22	46 x 10^{-3}

Deleted: of salt produced
Deleted: in-situ
Deleted: 24
Deleted: 332
Deleted: However, it is noteworthy that t
Deleted: of frazil ice concentration from salt inventories are anywhere from
Deleted: greater
Deleted: unquantified
Deleted: heat
Deleted: The influence of s
Deleted:
Deleted: s
Deleted: ¶
Deleted: salinity calculation does not account for
Deleted: However, evaporation could have contributed to excess salinity while simultaneously decreasing the temperature. …
Deleted: was secondary
Deleted: the
Deleted: so the effects of evaporation on salinity were likely therefore negligible. The effects of evaporation
Deleted: 48.85 x 10^{-3}
Deleted: 77.76 x 10^{-3}
Deleted: 16.42 x 10^{-3}
Deleted: --
Deleted: 22.59 x 10^{-3}
Deleted: 48.01 x 10^{-3}

28	May 06 17:59:12	0.007	15.52	18 x 10^{-3}	0.004	17.52	21 x 10^{-3}
29	May 07 15:29:32	0.004	11.34	22 x 10^{-3}	0.007	21.64	51 x 10^{-3}
30	May 09 07:28:24	0.007	8.24	25 x 10^{-3}	0.005	36.07	105 x 10^{-3}
32	May 09 18:24:56	0.008	11.33	32 x 10^{-3}	0.007	47.4	119 x 10^{-3}
33**	May 10 05:16:29	---	---	---	0.004	22.67	29 x 10^{-3}
34	May 10 20:16:46	0.004	13.4	9 x 10^{-3}	0.005	19.58	89 x 10^{-3}
35	May 11 00:56:32	0.012	19.58	35 x 10^{-3}	0.016	14.43	266 x 10^{-3}
40	May 17 04:02:37	0.006	20.61	33 x 10^{-3}	0.003	18.55	13 x 10^{-3}

Deleted: 17.85 x 10^{-3}
Deleted: 24.37 x 10^{-3}
Deleted: 22.05 x 10^{-3}
Deleted: 58.55 x 10^{-3}
Deleted: 24.88 x 10^{-3}
Deleted: 116.63 x 10^{-3}
Deleted: 32.39 x 10^{-3}
Deleted: 121.90 x 10^{-3}
Deleted: ---
Deleted: 32.38 x 10^{-3}
Deleted: 9.63 x 10^{-3}
Deleted: 80.29 x 10^{-3}
Deleted: 35.65 x 10^{-3}
Deleted: 332.16 x 10^{-3}
Deleted: 34.21 x 10^{-3}
Deleted: 48.84 x 10^{-3}

*Station 26 did not have a measurable salinity anomaly but was included due to the clarity of the temperature anomaly. Conversely, **Station 33 did not have a measurable temperature anomaly but was included due to the clarity of the salinity anomaly.

5.0 ESTIMATION OF TIME SCALE OF ICE PRODUCTION

How should we interpret the lifetime of these T and S anomalies? Are they short-lived in the absence of forcing, or do they represent an accumulation over some longer ice formation period? One possibility is that the anomalies begin to form at the onset of the katabatic wind event, implying that the time required to accumulate the observed heat and salt anomalies is similar to that of a katabatic wind event (e.g. 12-48 hours). This, in turn would suggest that the estimated

frazil ice production took place over the lifetime of the katabatic wind event. Another interpretation is that the observed anomalies reflect the near-instantaneous production of frazil ice. In this scenario, heat and salt are simultaneously produced and actively mixed away into the far field. In this case, the observed temperature and salinity anomalies reflect the net difference between production and mixing. One way to address the question of lifetime is to ask "if ice production stopped, how long would it take for the heat and salt anomalies to dissipate?" The answer depends on how vigorously the water column is mixing. In this section, we examine the mixing rate. However, we can first get some indication of the timescale by the density profiles.

Deleted: occurred

Deleted:

5.1 Apparent instabilities in the density profiles

Deleted: ¶

The computed density profiles reveal an unstable water column for all but one of our eleven stations (Figure 8). These suggest that buoyancy production from excess heat did not effectively offset the buoyancy loss from excess salt within each anomaly. It is not common to directly observe water column instability without the aid of microstructure or other instruments designed for measuring turbulence.

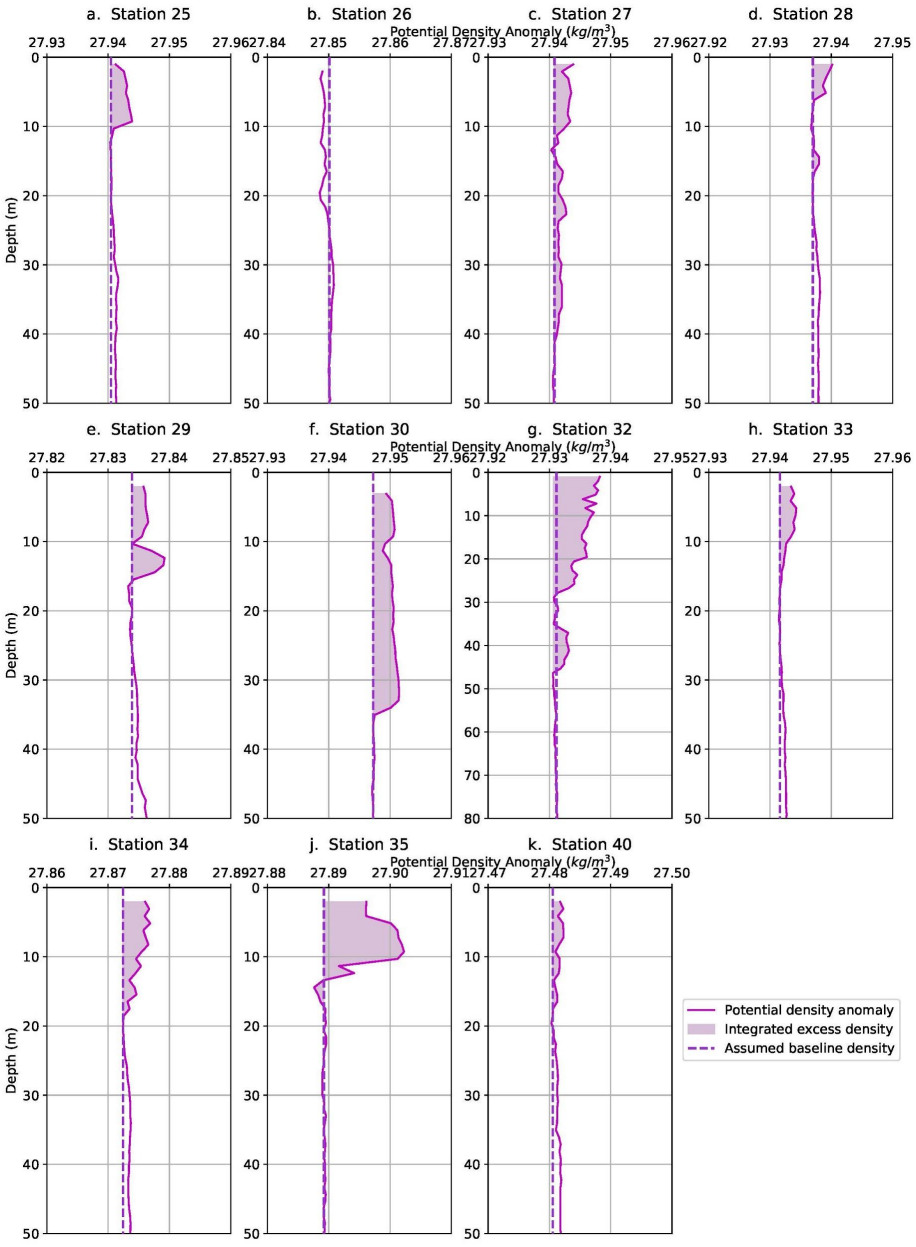
a. Station 25
b. Station 26
c. Station 27
d. Station 28
e. Station 29
f. Station 30
g. Station 32
h. Station 33
i. Station 34
j. Station 35
k. Station 40
Potential Density Anomaly (kg/m^3)
Depth (m)
Potential density anomaly
Integrated excess density
Assumed baseline density

817

Figure 8: Potential density anomalies for all 11 stations with evidence of active frazil ice formation. The integrated excess density and assumed baseline density are depicted to highlight the instability. Note that Station 26 (b) does not present a density anomaly because it does not have a salinity anomaly. In the absence of excess salinity, the temperature anomaly created instead an area of less dense water (i.e., a stable anomaly).

We suggest that an instability in the water column that persists long enough to be measured in a CTD profile, must be the result of a continuous buoyancy loss that is created at a rate faster than it can be eroded by mixing. In other words, the katabatic winds appeared to dynamically maintain these unstable profiles. Continuous ice production leads to the production of observed heat and salt excesses at a rate that exceeds the mixing rate. If the unstable profiles reflect a process of continuous ice production, then the inventory of ice that we infer from our simple heat and salt budgets must reflect ice production during a relatively short period of time, defined by the time it would take to mix the anomalies away, once the wind-driven dynamics and ice production stopped.

Similarly, Robinson et al (2014) found that brine rejection from platelet ice formation also leads to dense water formation and a static instability. Frazil ice formation from continually supplied Ice Shelf Water, formed from ice shelf melt and subject to pressure-induced supercooling, created a stationary instability, which was observable before being mixed by convection to the underlying homogeneous water column that extended to 200 meters (Robinson et al, 2020).

5.2 Lifetime of the salinity anomalies

` To estimate the lifetime of each salinity anomaly requires an estimate of the rate of turbulent mixing in the mixed layer. The Kolmogorov theory for turbulent energy distribution defines the eddy turnover time as the time it takes for a parcel to move a certain distance, d, in a turbulent flow (Valis, 2017). The smallest eddy scale is that of turbulent energy dissipation, and the largest scale is bounded by the length of the domain and the free stream turbulent velocity (Cushman-Roisin, 2019). This timescale can be estimated as,

Formatted: Font: Italic

Deleted: ¶

Formatted: Font: Italic

Formatted: Indent: First line: 0"

Deleted:

Deleted: 2017

Deleted: (§3.5)

Deleted: ISW

Deleted: Similarly, the katabatic winds and cold air temperatures continually supply supercooled water to the polynya supporting the instability.

Deleted: from Monin-Obukhov length scale

Formatted: Font: Italic

Formatted: Not Highlight

Deleted: Turbulence theory suggests energy that was injected largest scales by external forces excites the largest possible eddies and is gradually dissipated to smaller scalesthe largest eddies control the rate of turbulence dissipation …

Deleted: A

Deleted: In the energy cascade the rate at which energy was injected at the largest scales is equal to the rate at which it is dissipated at the smallest scales, which allows a characteristic timescale, t, can to be approximated by relating the largest eddy size and the rate of turbulent kinetic energy (TKE) dissipation (ε, Cushman-Roisin, 2019).

$$t \approx \frac{d}{(\varepsilon d)^{\frac{1}{3}}} \approx \left(\frac{d^2}{\varepsilon}\right)^{\frac{1}{3}} \quad (5)$$

Here, d is the characteristic length of the largest eddy and ε is the turbulent kinetic energy (TKE) dissipation rate, which is related to the free stream velocity as $\varepsilon \sim w^3/d$ (Cushman-Roisin, 2019). In this section we discuss and derive the best available estimates t using measurements of the meteorological forcing conditions and in-situ measurements of the turbulence.

If d is bounded only by the domain (in this case, the mixed layer depth), this would suggest vertical turbulent eddies up to 600 m in length (Table 2). However, a homogenous mixed-layer does not necessarily imply active mixing throughout the layer (Lombardo and Gregg, 1989). Instead, the length scale of the domain is more appropriately estimated from the size of the buoyancy instability and the background wind shear, or the Monin-Obukhov length (L_{M-O}) (Monin & Obukhov, 1954). When L_{M-O} is small and positive, buoyant forces are dominant and when L_{M-O} is large and positive, wind shear forces are dominant (Lombardo & Gregg, 1989). The L_{M-O} can be expressed the salt-driven buoyancy flux, reflecting the same process that gave rise to the observed salinity anomalies (see §4.3 for more detail).

$$L_{M-O} = -\frac{u_*^3}{k\beta g w \Delta S} \quad (6)$$

where u_* is the aqueous friction velocity, g is gravitational acceleration, w is the water vertical velocity, ΔS is the salt flux, β is the coefficient of haline contraction, and k is the von Karman constant. A more detailed explanation, along with the specific values are listed in Supplemental 4.

The friction velocity derives from the wind speed (U_{palmer}), measured at the NB Palmer weather mast from a height of z_{palmer} =24 m, adjusted to a 10 meter reference (U_{10}) (Manwell et al., 2010).

$$U_{10} = U_{palmer} \frac{ln(\frac{z}{z_o})}{ln(\frac{z_{palmer}}{z_o})} \quad (7)$$

Roughness class 0 was used in the calculation and has a roughness length of 0.0002 m. These values are used to estimate the wind stress as,

Deleted: 6
Formatted: Superscript
Deleted: discuss and select the best
Deleted: length scale for an environment dominated by buoyancy and wind shear. We use observed parameters to estimate the terms in equation (65)
Deleted: The
Deleted: dimension,
Deleted: , of the largest eddy in a vigorously mixing water column could be equivalent to the scale of the domain
Deleted: which was up to
Deleted: some of the PIPERS profiles
Deleted: characteristic length scale in an environment driven by both …
Deleted: is typically
Deleted: While t
Deleted: using several different estimates of shear and buoyancy, we focus on
Deleted: because those anomalies come closest to capturing the process of frazil ice production
Deleted: 7
Deleted: wind-driven
Deleted: at the water surface
Deleted: Wind-driven
Deleted: is estimated
Deleted: using the
Deleted: wind
Deleted: speed (U_{palmer}) record
Deleted: a masthead
Deleted: by assuming a logarithmic profile
Deleted: ∗
Deleted: 8

$$\tau = C_D \rho_{air} U_{10}^2 \quad (8)$$

where ρ_{air} represents the density of air, with a value of 1.3 kg m^{-3} calculated using averages from NB Palmer air temperature (-18.7 °C), air pressure (979.4 mbars) and relative humidity (78.3%). C_D, the dimensionless drag coefficient, was calculated as 1.525 x 10^{-3} using the NOAA COARE 3 model, modified to incorporate wave height and speed (Fairall et al, 2003). The average weather data from NB Palmer was paired with the wave height and wave period from the SWIFT deployment (defined below) on 04 May to find C_D. A more detailed explanation and the specific values are listed in Supplemental 5. Finally, u_* from equation (6) is:

$$u_* = \sqrt{\frac{\tau}{\rho_{water}}} \quad (9)$$

During the katabatic wind events, a SWIFT (Surface Wave Instrument Float with Tracking) buoy was deployed to measure TKE dissipation and vertical velocity, w, and wave field properties. (Thomson et al, 2016; Zippel & Thomson, 2016). SWIFT deployments occurred within the period of CTD observations, as shown in the timeline of events (Supplemental Figure 5), however they do not coincide in time and space with the CTD profiles. For the vertical velocity estimation, we identified the May 04 and May 09 SWIFT deployments as most coincident to CTD stations analyzed here, based on similarity in wind speeds. The average wind speed at all the CTD stations with anomalies was 10.2 m s^{-1}. For the May 4 SWIFT deployment, the wind speed was 9.36 m s^{-1}. CTD Station 32 experienced the most intense sustained winds of 18.9 m s^{-1}. The May 9 SWIFT deployment was applied to CTD 32, which had a wind speed of 20.05 m s^{-1}. During these SWIFT deployments, the average vertical velocity (w) was measured in the upper meter of the column. May 04 had an average value of w= 0.015 m s^{-1}. May 09 had an average value of w= 0.025 m s^{-1}. See Thomson et al., (2016) & Zippel & Thomson, (2016) for details on how these measurements are made.

The TKE dissipation rates are expected to vary with wind speed, wave height, ice thickness and concentration (Smith & Thomson, 2019). Wind stress is the source of momentum to the upper ocean, but this is modulated by scaling parameter (c_e, Smith & Thomson, 2019). If the input of TKE is in balance with the TKE dissipation rate over an active turbulent layer, the following expression can be applied:

$$c_e \tau \propto \rho \int \varepsilon(z)\, dz \quad (10)$$

Deleted: 9
Deleted: ¶
Deleted: 406
Deleted: 3
Deleted: represents
Deleted: a
Deleted: and
Deleted: ,
Deleted: code
Deleted: ¶
¶
We determined the aqueous friction velocity (
Deleted:)
Deleted: at th
Deleted: e air-sea interface using
Deleted: 10
Deleted: We used a
Deleted: provide estimate
Deleted: s of turbulent kinetic energy
Formatted: Font: Italic
Formatted: Font: Not Italic
Deleted: .
Deleted: during
Deleted: 3
Deleted: .
Deleted: The SWIFT deployments
Deleted: always
Deleted: estimation
Deleted: relevant
Deleted: , more than two standard deviations from the
Deleted: average, experienced the most intense winds of the CTD stations at 18.9 m s-1
Deleted: . For CTD Station 32, t
Deleted: used
Deleted: For May 04 and May 09, the
Formatted: Font: Italic
Deleted: (τ_{wind})
Deleted: depth layer,
Deleted: *
Deleted: *wind*
Deleted: 1

where the density of water (ρ) is assumed to be 1027 kg m^{-3} for all stations. This scaling parameter incorporates both wave and ice conditions; more ice produces more efficient wind energy transfer, while simultaneously damping surface waves, with the effective transfer velocity in ice, based on the assumption that local wind input and dissipation are balanced Smith & Thompson (2019) used the following empirical determination of c_e:

$$c_e = a\,(A\,\frac{z_{ice}}{H_s})^b \qquad (11)$$

Here, A is the fractional ice cover, with a maximum value of 1, z_{ice} is the thickness of ice, and H_s is the significant wave height. Using Antarctic Sea ice Processes and Climate or ASPeCt visual ice observations (www.aspect. aq) from NB Palmer, the fractional ice cover and thickness of ice were found at the hour closest to both SWIFT deployments and CTD profiles (Knuth & Ackley, 2006; Ozsoy-Cicek et al., 2008; Worby et al., 2008). SWIFT wave height measurements yielded an average value of H_s = 0.58 m for May 04, and this value was applied to all the CTD profiles. To obtain the most robust data set possible, in total, 13 vertical SWIFT profiles from May 2, May 4, and May 9 were used to evaluate equation 12 over an active depth range of 0.62 meters.

Using the estimates of c_e, τ, and ε from the SWIFT, we parameterized the relationship between wind stress and ε that is reflected in equation (11). A linear fit on a log-log scale ($y = 10^{(1.4572\,log10(x)\,+0.2299)}$, r^2= 0.6554) was then applied to NB Palmer wind stress data to derive turbulent kinetic dissipation estimates that coincided with the ambient wind conditions during each CTD station (Table 2).

Formatted: Indent: First line: 0"
Formatted: Font: Italic
Deleted: e
Deleted: Smith & Thompson,
Deleted: ¶
Formatted: Font: Italic
Formatted: Font: Italic, Subscript
Deleted: .
Deleted: 2
Formatted: Font: Italic
Deleted: age of ice
Deleted: ,
Formatted: Font: Italic
Deleted:
Formatted: Font: Italic
Deleted: The significant wave height for each SWIFT deployment was used. We lacked time series data
Commented [BL6]: Why only use wave data from May 4?
Formatted: Font: Italic
Formatted: Font: Italic, Subscript
Deleted: for H_s during the time of CTD casts, so the
Deleted: average value from May 04 of 0.58 m
Deleted: was used for
Deleted: get
Formatted: Not Highlight
Deleted: ¶
Deleted: τ
Deleted: log-linear
Deleted: *

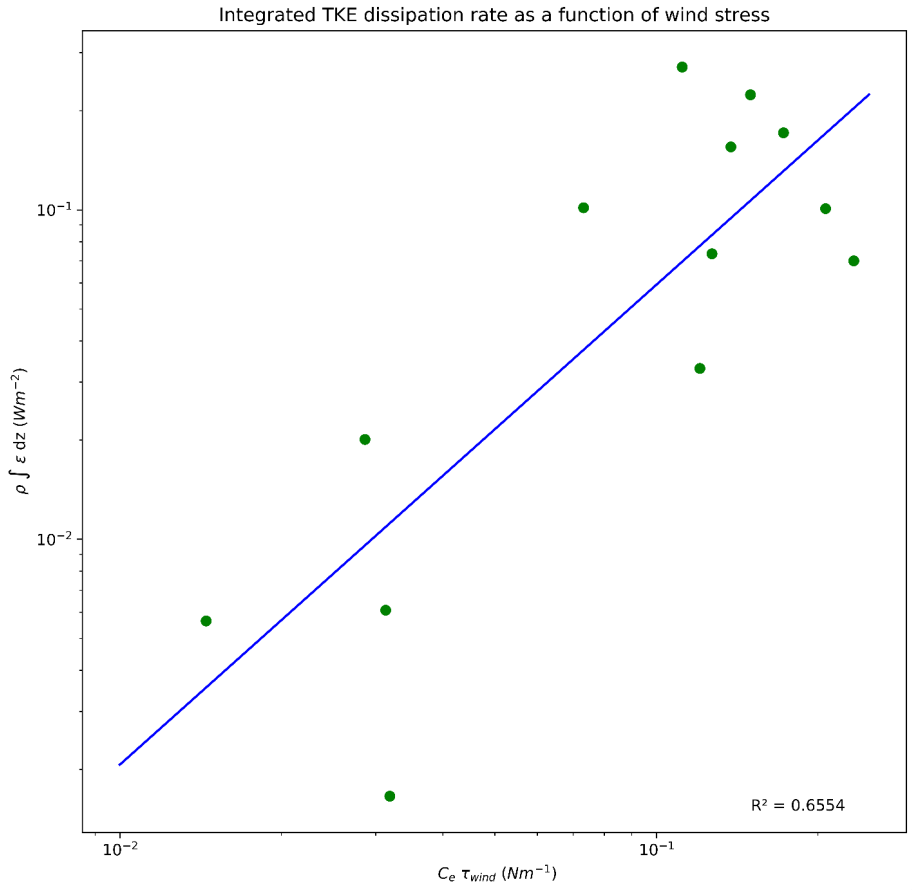

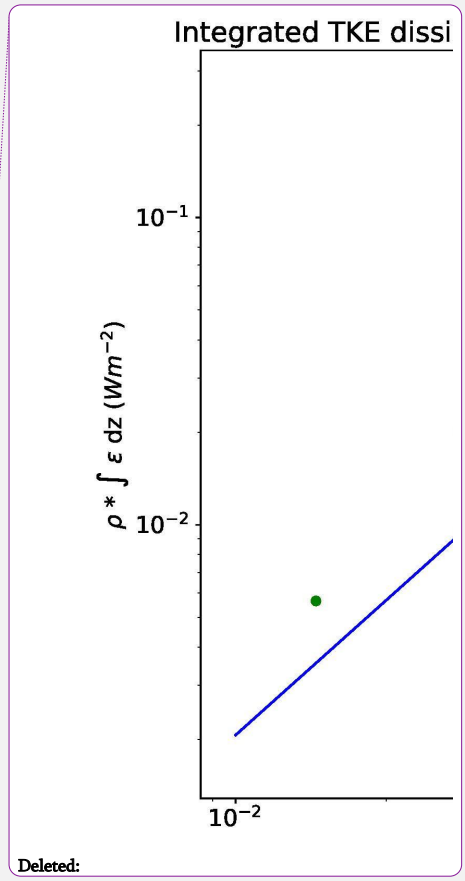

Deleted:

Figure 9: Input wind-driven TKE into the surface ocean versus the TKE dissipation rate over the active depth range. A linear scaling relationship was applied to the log of each property.

Deleted: Logarithmic linear fit

Deleted: A linear fit on a log-log scale of the i

Deleted: flux of

Gathering these estimates of w, u_* and ε, we have the necessary elements to estimate the anomaly lifetime using equation (5). Because L_{M-O} has been chosen to represent the domain length scale, we rewrite equation (6) as:

Formatted: Subscript

Formatted: Not Superscript/ Subscript

$$t = \left(\frac{L_{M-O}^2}{\varepsilon}\right)^{\frac{1}{3}} \qquad (12)$$

Moved (insertion) [1]

Deleted: $\frac{\pi \, d}{v_*} \approx \frac{d}{(\varepsilon \, d)^{\frac{1}{3}}} \approx$

Deleted: → t =timescale= s¶
ε =turbulent kinetic energy dissipation= 1.85 x 10^{-5}m^2 s^{-3} ¶
L_{M-O}= Monin-Obukhov Length= m ¶

Haline contraction, β, in equation (6), was calculated from Gibbs Seawater toolbox and averaged over the depth range of the anomaly. The excess salt, ΔS, was found using the average value of ΔS for each profile anomaly. The values of L_{M-O} range from 6 m to 330 m (Table 2). In general, L_{M-O} was greater than the length of the salinity anomaly but smaller than the mixed layer depth. $t = \frac{\pi d}{v_*} \approx \frac{d}{(\varepsilon d)^{\frac{1}{3}}} \approx \left(\frac{L_{M-O}{}^2}{\varepsilon}\right)^{\frac{1}{3}} \varepsilon = L_{M-O}$

The mixing lifetime of these salinity anomalies ranged from 2 to 12 minutes, but most values cluster near the average of 9 min. The average timescale is similar to the frazil ice lifetime found in Michel (1967). **These lifetimes suggest that frazil ice production and the observed density instabilities relax to a neutral profile within ten minutes of a diminution in wind forcing.**

6.0 RATE OF FRAZIL ICE PRODUCTION

We can extend the analysis of anomaly lifetime to estimate the frazil ice production rate. Heuristically, the lifetime of the anomaly is equivalent to the time it would take for the anomaly to be dissipated, or *produced*, given the observed conditions of heat loss to the atmosphere. By that analogy, the sea ice production rate is,

$$Production\ rate = \frac{Conc_{ice}^{salt}\ z_S}{t\ \rho_{ice}} \quad (13)$$

Here, $\rho_{ice} = 920$ kg m^{-3} and z_s =the depth of the salinity anomaly (m). The results are summarized in Table 2. A more detailed explanation and the individual terms from equation 13 are listed in Supplemental 6. To capture the uncertainty in the sea ice production rates, we used the Student t-distribution to derive confidence intervals (CI) for TKE dissipation rate at each CTD station was used to bound the range of ice production rates, which are reported in Table 2. Uncertainty in the heat and salt inventories were not included in the uncertainty estimates, because we observed negligible difference in the inventory while testing the inventory for effects associated with bin averaging of the CTD profiles (Section 2.3). Another small source of error arises from the neglect of evaporation. To quantify the amount of error introduced by that assumption, we used the bulk aerodynamic formula for latent heat flux and found the effects of evaporation across the CTD stations to be 1.8% [0.07-3.45%] (Zhang, 1997).This error due to the effects of evaporation found are similar to Mathiot et al (2012). On average, the lower limit

Deleted: Following estimation of the environmental parameters, Equation 7 can now be used to estimate L_{M-O}.. For these calculations a value of 0.41 was used for the von Karman constant, k.

Deleted: , β,

Moved up [1]: $t = \frac{\pi d}{v_*} \approx \frac{d}{(\varepsilon d)^{\frac{1}{3}}} \approx \left(\frac{L_{M-O}{}^2}{\varepsilon}\right)^{\frac{1}{3}}$ (12)¶
t =timescale= s¶
ε =turbulent kinetic energy dissipation= 1.85 x 10^{-5}m^2 s^{-3} ¶
L_{M-O}= Monin-Obukhov Length= m ¶

Deleted: Using L_{M-O} and the estimates of ε, the characteristic lifetimetimescale *(t)* Equation 5 can be rewritten and solved as:¶

Deleted: The characteristic timescale shows us that the

Deleted:

Formatted: Font: Bold

Deleted: ¶

Deleted: a

Deleted: by invoking the prior assumption of steady state TKE forcing and dissipation.

Formatted: Font: Italic

Deleted: In this case, the mass of ice reflected by the salinity anomaly ($Conc_{ice}^{salt}$, in kg m^{-3}) was produced during the time interval corresponding to the mixing lifetime

Deleted: (t) that was determined from TKE dissipation in §5.2….

Deleted: .

Deleted: *

Deleted: *

Deleted: 3

Deleted: , t=timescale/lifetime, in days

Deleted:

Deleted: specific

Deleted: values

of ice production was 30% below the estimate and the upper limit was some 44% larger than the estimated production.

The estimates of frazil ice production rate span two orders of magnitude, from 3 to 302 cm d^{-1}, with a median ice production is 25 cm d^{-1}. The highest ice production estimate occurred at CTD 35, closest to the Antarctic coastline and the Nansen Ice Shelf. The next largest value is 110 cm d^{-1}, suggesting the ice production at CTD 35 is an outlier, and may be a consequence of platelet ice in upwelling ice shelf water (Robinson et al., 2014). Here forward, we will exclude the ice production rate at CTD 35 from the trend analysis.

The remaining ice production rates, span a range from 3 to 110 cm d^{-1} and reveal some spatial and temporal trends that correspond with the varying conditions in different sectors of the TNB polynya. A longitudinal gradient emerges along the length of the polynya, when observing a subset of stations, categorized by similar wind conditions CTD 30 (U_{10}=11.50 m s^{-1}), CTD 27 (U_{10}=10.68 m s^{-1}), and CTD 25 (U_{10}=11.77 m s^{-1}). Beginning upstream near the Nansen Ice shelf (Station 30) and moving downstream along the predominant wind direction toward the northeast, the ice production rate decreases. The upstream production rate is 63 cm day^{-1} followed by midstream values of 28 cm day^{-1}, and lastly downstream values of 14 cm day^{-1}.

The spatial trend we observed somewhat mimics the 3D model of TNBP from Gallee (1997). During a four-day simulation, Gallee found highest ice production rates near the coast (e.g. our Station 35) of 50 cm day^{-1}, and decreased to 0 cm day^{-1} downstream and at the outer boundaries, further west than PIPERS Station 33 (Figure 10). While some of the ice production rates derived from PIPERS CTD profiles exceed prior results, we attribute that excess to the relatively short time scale of these ice production "snapshots". These estimates integrate over minutes to tens of minutes, instead of days to months, therefore they are more likely to capture the high frequency variability in this ephemeral process. As the katabatic winds oscillate, the polynyas enter periods of slower ice production, driving average rates down.

Table 2: Summary of mass of ice derived from salinity, lifetime, and production rates.

Deleted: ¶
¶
6.1 Variability in the frazil ice production rate ¶

Deleted: ten

Deleted: , expressed as ice thickness per unit time, ranged

Deleted: 7

Deleted: 78

Deleted: ay

Deleted: . Th

Formatted: Superscript

Deleted: ese frazil ice production rates show some spatial trends across the Terra Nova Bay polynya

Deleted: variable

Deleted: environmental

Deleted: s shown in Figure 10, a

Deleted: axis of the TNBP

Deleted: looking at

Deleted: subsection

Deleted: under

Deleted: Station

Deleted: Station

Deleted: Station

Deleted: the predominant

Deleted: 9.38

Deleted: .43

Deleted: 9.83

Deleted: This pattern is similar to the pattern modeled by Gallee (1997). …

Deleted: The production

Formatted: Indent: First line: 0.5"

Deleted: The production rate at Station 35, was significantly higher than that at all other stations, but this large excess is reflected in both the heat and salt anomalies. The salt inventory at station 35 is35 is a factor of 32.6 greater than the nearest station (Station 34), and profiles 34 and 35 were separated in time by less than 5 hours .hours. This other variations in ice production rate may reflect real variability brought on by submesoscalesub mesoscale fronts, eddies and other flow structures that are not easily captured by coarse sampling. …

Deleted: The longitudinal gradient moving downstream the polynya can be used to extrapolate an average monthly ice production rate. As shown in figure 10 with the blue dashed line, a parallelogram was built around the area of active frazil ice formation observed and serves as an estimate for surface area. The surface area depicted, 3400 km2, exceeds … [11]

Deleted: We used the student t-distribution to derive … [12]

Station	$Conc_{ice}^{S}$ (kgm^{-3})	z_s (m)	L_{M-O} (m)	TKE diss. ε (m^2 s^{-3})	MLD (m)	Timescale/ Lifetime *(t)* (min)	Production rate (cm day^{-1})	Production rate 95% CI (cm day^{-1})
25	67 x 10^{-3}	13.4	141	9.648 x 10^{-5}	350	9.8	14	[10 - 20]
26*	--	--	--	7.191 x 10^{-5}	100	---	---	--
27	46 x 10^{-3}	41.2	151	8.188 x 10^{-5}	500	10.9	28	[20- 37]
28	21 x 10^{-3}	17.5	54	1.622 x 10^{-5}	600	9.4	6	[4- 10]
29	51 x 10^{-3}	21.6	80	5.375 x 10^{-5}	275	8.2	21	[15 - 28]
30	105 x 10^{-3}	36	83	3.771 x 10^{-5}	500	9.5	63	[45- 88]
32	119 x 10^{-3}	47	198	3.466 x 10^{-4}	375	8.0	110	[67-181]
33	29 x 10^{-3}	23.7	98	2.844 x 10^{-5}	500	11.6	9	[5- 13]
34	89 x 10^{-3}	19.6	66	6.397 x 10^{-5}	175	6.8	31	[23 - 42]
35	266 x 10^{-3}	14.4	6	2.343 x 10^{-5}	150	2.0	302	[200- 456]
40	13 x 10^{-}	18.6	175	9.603 x	120	11.7	3	[2- 5]

Deleted: Est
Formatted Table ... [13]
Formatted ... [14]
Deleted: 0.59
Deleted: 9.83
Deleted: 16.60
Deleted: [12.16 - 22.66]
Deleted: 77.76 x 10^{-3}
Deleted: ^{0}
Deleted: --
Deleted: --
Deleted: --
Deleted: --
Deleted: ^{0}
Deleted: .26
Deleted: 10.90
Deleted: 28.43
Deleted: [20.98 - 38.51]
Deleted: 48.01 x 10^{-3}
Deleted: ^{0}
Deleted: .12
Deleted: 9.42
Deleted: 7.09
Deleted: [4.40 - 11.45]
Deleted: 24.37 x 10^{-3}
Deleted: ^{0}
Deleted: .00
Deleted: 8.20
Deleted: 24.19
Deleted: [17.75 - 32.96]
Deleted: 58.55 x 10^{-3}
Deleted: ^{0}
Deleted: .45
Deleted: 9.49
Deleted: 69.38
Deleted: [49.34 - 97.55]
Deleted: 116.63 x 10^{-3}
Deleted: ^{0}
Deleted: 7.03
Deleted: 8.03
Deleted: 112.57
Deleted: [68.25 -185.69]
Deleted: 121.90 x 10^{-3}
Deleted: ^{0}
Deleted: .38
Deleted: 11.64
Deleted: 9.87
Deleted: [6.76 - 14.43]
Deleted: 32.38 x 10^{-3}
Deleted: ^{0}
Deleted: 5.5
Deleted: 6.78
Deleted: 36.31
Deleted: [26.83 - 49.14]
Deleted: 80.29 x 10^{-3}
Deleted: ^{0}
Deleted: .30
Deleted: 1.99

	3			10^{-5}				

*Station 26 did not have a measurable salinity anomaly but was included due to the clarity of the temperature anomaly. The term MLD stands for estimated mixed layer depth.

6.1 Seasonal Ice Production

We can estimate the seasonal average in sea ice production by relating these in-situ ice production estimates to the atmospheric forcing. The sensible heat flux (Q_s), measured at the automated weather station Manuela, was used to empirically scale the ice production rates.

$$Q_s = c_p \rho_a C_s u_{10} (T_b - T_a) \quad (14)$$

here c_p= 1.003 kJ kg^{-1} K^{-1}, the specific heat capacity of air at -23 ◦C, C_s= 1.297 X 10^{-3}, is the heat transfer coefficient calculated using the COARE 3.0 code (Fairall et al, 2003). The values are included in Supplemental Table S6.

The sensible heat flux was calculated using NB Palmer meteorological data, from times coinciding with the TNBP CTD stations. Station 35 (see §5.1) and Station 40, in the Ross Sea Polynya, were excluded from this calculation. Figure 11 depicts the trend between Q_s and sea ice production rate; the high degree of correlation (R^2 = 0.915) likely occurs because the same NB Palmer wind speeds were used in the calculation of both Q_s and sea ice production (equation 7); in other words, the two terms are not strictly independent of each other.

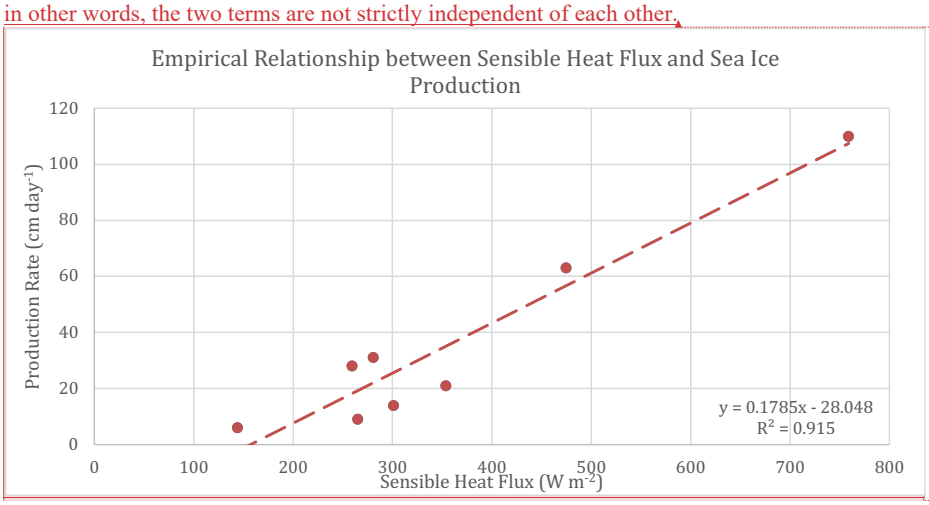

Figure 11: Empirical relationship between sensible heat flux and sea ice production: Production rate = 0.1785 Q_s -28.048, R^2 of 0.915.

The met data from the NB Palmer and from Station Manuela (Figure 3) reveal that TNBP experiences slower wind speeds and warmer temperatures than Station Manuela. This phenomenon has been explained as a consequence of adiabatic warming and a reduction in the topographic 'Bernoulli' effects that cause wind speed to increase at Station Manuela (Schick,

Deleted: 48.84 x 10^{-3}
Deleted: 0
Deleted: EST
Deleted: =
Deleted: ¶
Formatted: Font: Italic
Formatted: Font: Italic, Subscript
Formatted: Indent: First line: 0.5"
Commented [LDP10]: Sta 38 is not one of our stations
Formatted: Font:
Commented [BL11]: This should probably go as a small figure in the manuscript
Commented [BL12]: This doesn't need to be reported in the text, but can be shown in the Figure and should be reported in the figure caption.
Commented [BL13]: This is already in the ms
Formatted: Font: Italic
Formatted: Font: Italic, Subscript
Commented [LDP14]: Figure 3 n MS

2018). Before relating the time series of Q_s from Manuela to the values of Q_s computed for each CTD Station, we needed to account for the offset. The air temperatures were 6.5 ◦C warmer, and wind speed was on 7.5 m s^{-1} slower in TNB, during the 13 days that the vessel was in the polynya, and these average differences were removed from the time series of Q_s from Manuela. Figure S6.1 shows the corrected data against the original data.

We estimated the seasonal average in Q_s over TNBP using the corrected met data from Station Manuela, and an average sea surface temperature from the CTD stations (-1.91 °C), the air density, specific heat capacity, and heat transfer coefficient remained the same as above. The average in Q_s from April to September is 321 W m^{-2}. Using the empirical relationship described in Figure 11, the seasonal average ice production rate is 29 cm day^{-1}.

The seasonal sea ice production rate varies based on many factors affecting the rate of heat loss from the surface ocean. These factors include a strong negative feedback between ocean heat loss and sea ice cover. As the polynya builds up with ice, heat fluxes to the atmosphere will decline (Ackley et al, 2020 in review) until that ice cover is swept out of the polynya by the next katabatic wind event. This spatial variation in ice cover and wind speed, produces strong spatial gradients in the heat loss to the atmosphere that drives ice production. For example, Ackley et al., (Figure 3, 2020 in review) observed heat flux variations from nearly 2000 W m^{-2} to less than 100 W m^{-2} over less than 1 km. An integrated estimate of total polynya sea ice production should take these spatial gradients and the changes in polynya area into account. That analysis is somewhat beyond the scope of this study, but we anticipate including these ice production estimates within forthcoming sea ice production estimates for 2017 and PIPERS.

One interesting outcome of the scaling relationship in Figure 11, is the value of the y-intercept at 157 W m^{-2}. This relationship suggests that frazil ice production ceases when the heat flux falls below this range. This lower bound, in combination with the spatial gradients in heat flux may help to establish the region where active production is occurring.

6.1 Comparison to prior model and field estimates of ice production

The 29 cm d^{-1} of seasonal average ice production that we estimated here, falls within the range of other in-situ ice production estimates. Schick (2018) estimated a seasonal average ice production rate of 15 cm day^{-1}, and Kurtz and Bromwich (1985), determined 30 cm day^{-1}. Both studies derived their ice production rates using a heat budget.

Overall, these ice production estimates from in-situ data are larger than the seasonal production estimates derived from remote sensing products. Drucker et al (2011) used the AMSR-E instrument to obtain a seasonal average of 12 cm day^{-1} for years 2003-2008. Oshima et al, (2016) estimated 6 cm day^{-1} of seasonal production for the years 2003-2011, and Nihashi and Ohshima (2015) determined 7 cm day^{-1} for years 2003-2010. Finally, Tamura et al (2016) found production rates that ranged from 7-13 cm day^{-1}, using both ECMWF and NCEP Reanalysis products, reflecting a greater degree of consistency in successive estimates, likely because of consistency in the etimation methods.

In comparison, the modeling studies tend to skew higher than the in-situ observations: Sansiviero et al (2017) estimated 48 cm day^{-1} using a sea-ice model. Petrelli, Bindoff, &

Formatted: Font: Italic
Formatted: Font: Italic, Subscript
Formatted: Font: Italic
Commented [LDP15]: Text moved to supplemental 6
Commented [BL16]: This can be a supplemental figure. This figure is slightly problematic because it shows a negative windspeed.
Formatted: Font: Italic, Subscript
Formatted: Indent: First line: 0.5"
Formatted: Font: Italic
Commented [LDP17]: Not sure how to cite this. I checked the reference section of cryosphere website and couldn't figure it out
Formatted: Superscript
Formatted: Not Highlight
Formatted: Indent: First line: 0"
Deleted: 2
Deleted: Calculated production rates from PIPERS ranged from 3 to 3027 to 378 cm day^{-1} (Figure 10)
Formatted: Superscript
Deleted: . The median ice production rate, 286.31 cm day^{-1}, is similar to
Deleted: , who
Deleted: n
Deleted: ,
Deleted: 16.8
Deleted: for the month of May, (calculated using atmospheric heat fluxes). Our median is also similar to
Deleted: ,
Deleted: who also used a heat budget to estimate an average ice production rate of 30 cm day^{-1} for the month of May.
Formatted: Line spacing: Multiple 1.15 li
Formatted: Font: Not Bold
Formatted: Font:
Formatted: Line spacing: 1.5 lines
Deleted: All of these estimates are smaller than the winter average from
Deleted: of
Deleted: .08

Bergamasco (2008) modeled a wintertime maximum production rates of 26.4 cm day^{-1} using a coupled atmospheric-sea ice model. Fusco et al (2002) applied a model for latent heat polynyas and modeled production rate at 85 cm day^{-1} for 1993 and 72 cm day^{-1} for 1994.

It is worth noting that our production estimate applies to only frazil ice, rather than total ice production. Columnar ice growth, for example, is usually considered the predominant ice type in overall ice production, suggesting that our method implies a larger value for total ice production during one season. However, the large range of ice production estimates cited above, and the clustering of estimates from (1) in-situ data, from (2) remote sensing data, and from (3) models in ranges that do not overlap, suggests a comparison of methods may be helpful to achieve consistency and a convergence in estimates.

Commented [BL19]: Can you confirm we 're comparing apples to apples? We want the average, if they provided it.

Formatted: Highlight

Commented [BL20]: Are these maxima or seasonal avgs?

Formatted: Font:

Commented [BL21]: This paragraph should be revised if the modeling values you cite are not seasonal averages.

Deleted: ¶
The spatial trend we observed somewhat mimics the model 3D model of TNBP from Gallee (1997) . During a four-day simulation, Gallee found highest ice production rates near the coast (e.g. our Station 35) of 50 cm day^{-1}, and decreasing production to 0 cm day^{-1} downstream and at the outer boundaries, further west than PIPERS Station 33 (Figure 10). While some of the ice production rates derived from PIPERS CTD profiles exceed prior results, we attribute that excess to the relatively short time scale of these ice production "snapshots". These estimates integrate over minutes to tens of minutes, instead of days to months, therefore they are more likely to capture the high frequency variability in this ephemeral process. As the katabatic winds oscillate, the polynyas enter periods of slower ice production, driving average rates down. ¶
Our median production rate can be scaled over the average size of the polynya (1300 km2) and a season of March to October to find an annual production rate. The annual production rate is 76 km3 per year. In review of Drucker et al, 2011, they used Advanced Microwave Scanning Radiometer-EOS (AMSR-E) to find the average production rate of 88 km3. Oshima et al, (2016) used satellite remote sensing using passive microwave sensors to find the average production rate of 53 km3. Nihashi and Ohshima (2015) used passive microwave sensing to find the average production rate of 59 km3.¶

Formatted: Indent: First line: 0"

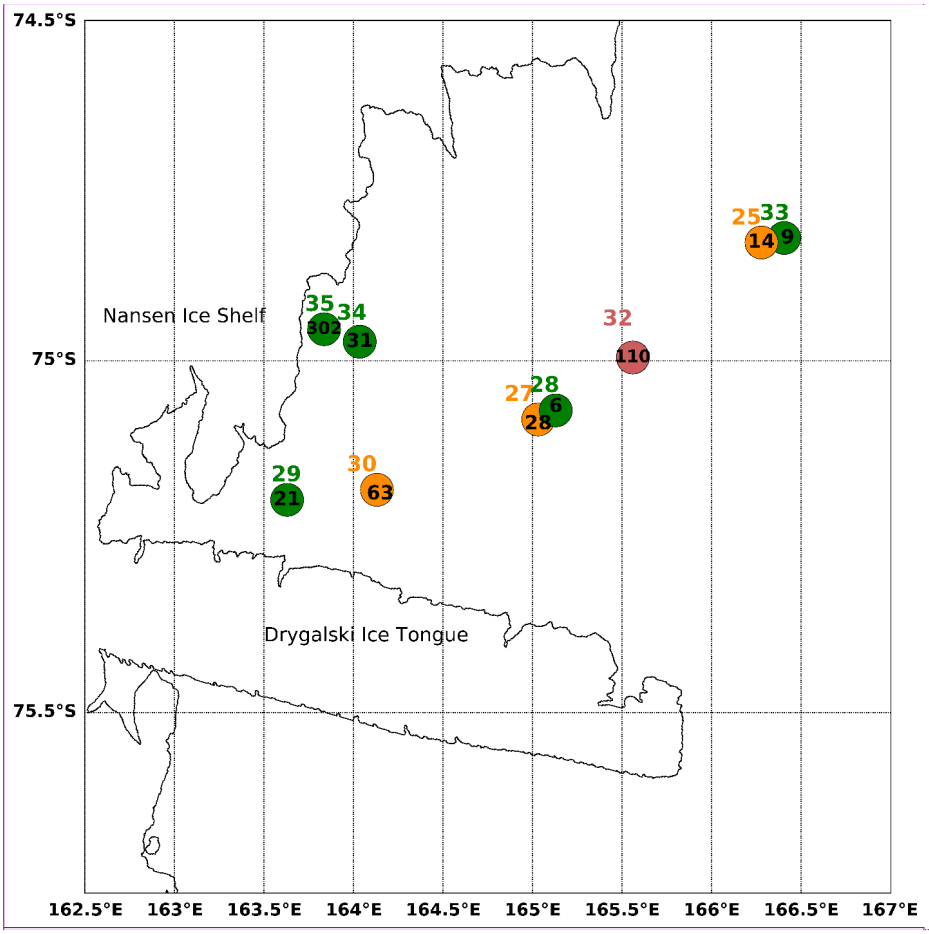

Figure 10: TNBP map of ice production rates. Map of TNBP CTD stations with anomalies and ice production rates. The CTD station number is listed in to the north of the stations. Listed inside the circle in black is the respective ice production rate in cm day^{-1}. The symbols and station numbers are colored by wind speed: Green indicates wind speeds less than 10 m s^{-1} (Stations 28, 29, 33, 34, 35), Orange indicates wind speeds between 10 and 15 m s^{-1} (Stations 25, 27, 30), and Red indicated wind speeds over 15 m s^{-1} (Station 32).

7. CONCLUSIONS

Commented [LDP22]: I prefer this presentatio

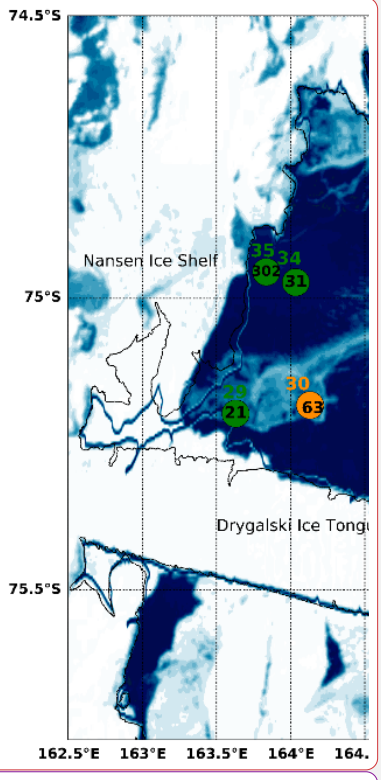

Deleted:

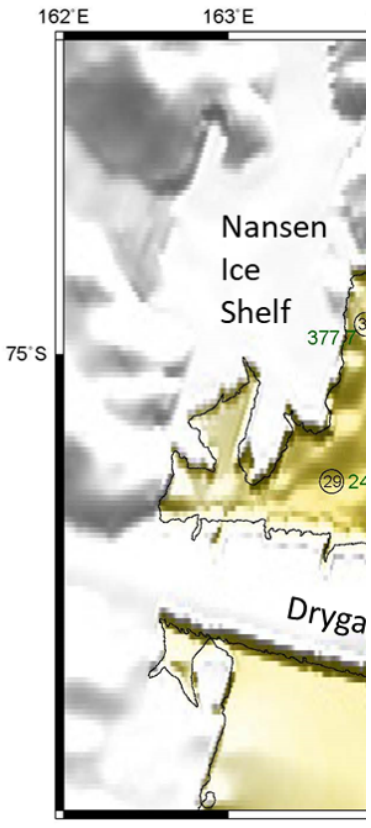

Deleted: ... [15]

Polynyas have been regarded as ice production factories with a wide range of modeled production rates. During a late autumn oceanographic expedition to the Ross Sea, PIPERS acquired CTD profiles in the ocean during strong katabatic wind events in both the Terra Nova Bay polynya and the Ross Sea polynya. In those profiles we found near surface temperature and salinity anomalies, which provided a new method for quantifying ice production rates in-situ. Salinity and temperature anomalies observed at 11 CTD stations indicated frazil ice formation and were used to estimate polynya ice production. Our estimated frazil ice production rates varied from 3 to 110 cm day^{-1}. This wide range of estimates captures frazil ice production on very on the timescale of tens of minutes. We note that the robustness of these estimates could be improved by collecting consecutive CTD casts at the same location. One exciting outcome of this study is the suggestion that it is possible to obtain synoptic inventories of ice production. For example, a float or glider that is designed to gather surface CTD profiles on a frequent basis, could thereby improve synoptic and seasonal estimates of polynya ice production as it responds to annual and secular modes of the ocean and atmosphere.

Formatted: Line spacing: 1.5 lines

Deleted: 7

Deleted: 302

Deleted: 78

Deleted: e

Deleted: is likely

Deleted: ing

Deleted: short timescales (

Deleted:)

Deleted: collecting consecutive

Deleted: ¶
The polynyas in the Ross Sea show high ice production rates and are significant contributors to Antarctic Bottom Water formation. Since 2015, sea ice extent around Antarctica has decreased, with 2017 being an abnormally low year (Supplemental Figure 56; Fetterer et al, 2017).

Formatted: Font:

Deleted: One of the goals of PIPERS was to understand if sea ice extent in the Ross Sea was controlled primarily by ice production at the coast. If true, the decreased ice extent in recent years may be related to changes in ice production in the polynyas. To further address these questions, our estimates of polynya ice production can be paired with other ice products derived from remote sensing, such as ice thickness from airborne and satellite lidar and ice area from radar and passive microwave to better address the observed year-to-year changes. A decrease in ice production rate correlates to freshening of Antarctic bottom water which would have global impacts. ¶

8. REFERENCES

Ackley, S.F. Ackley[1], Stammerjohn, S., Maksym, T. Smith, M., Cassano, J., Guest P. Tison, J-L., Delille, B. Loose, B., Sedwick, P. DePace, L., Roach, L., Parno, J. (2020 in review) Sea ice production and air-ice-ocean-biogeochemistry interactions in the Ross Sea during the PIPERS 2017 autumn field campaign. Annals of Glaciology.

Deleted: ¶

Formatted: Indent: Left: 0", First line: 0"

Armstrong, T.: World meteorological organization: wmo sea-ice nomenclature. terminology, codes and illustrated glossary, J. Glaciol., 11, 148-149, https://doi-org.uri.idm.oclc.org/10.3189/S0022143000022577, 1972.

Bromwich, D. H., and Kurtz, D. D.: Katabatic wind forcing of the terra nova bay polynya, J. Geophys. Res., 89, 3561-3572, https://doi-org.uri.idm.oclc.org/10.1029/JC089iC03p03561, 1984.

Buffoni, G., Cappelletti, A., and Picco, P.: An investigation of thermohaline circulation in terra nova bay polynya, Antarct. Sci, 14.1, 83-92, https://doi-org.uri.idm.oclc.org/10.1017/S0954102002000615, 2002.

Cosimo J.C., and Gordon A.L.: Inter-annual variability in summer sea ice minimum, coastal polynyas and bottom water formation in the weddell sea, in: Antarctic sea ice: physical processes, interactions and variability, 74, edited by: Jeffries, M.O., American Geophysical Union, Washington, D.C., 293-315, https://doi.org/10.1029/AR074p0293, 1998.

Cox, G. F. N., and Weeks, W. F.: Equations for determining the gas and brine volumes in sea-ice samples, J. Glaciol., 29, 306-316, https://doi.org/10.3189/S0022143000008364, 1983.

Cushman-Roisin, B.: Environmental Fluid Mechanics, John Wiley & Sons, New York, 2019.

Dmitrenko, I. A., Wegner, C., Kassens, H., Kirillov, S. A., Krumpen, T., Heinemann, G., Helbig, A., Schroder, D., Holemann, J.A., Klagger, T., Tyshko, K.P., and Busche, T.: Observations of supercooling and frazil ice formation in the laptev sea coastal polynya, J. Geophys. Res., 115, https://doi-org.uri.idm.oclc.org/10.1029/2009JC005798, 2010.

Drucker, R., S. Martin, and R. Kwok: Sea ice production and export from coastal polynyas in the Weddell and Ross Seas. Geophys. Res. Lett., 38, L17502, https://doi.org/10.1029/2011GL048668m, 2011.

Fairall, C.W., Bradley, E.F., Hare, J.E., Grachev, A.A., and Edson, J.B.: Bulk parameterization of air sea fluxes: updates and verification for the COARE algorithm, J. Climate, 16, 571-590, https://doi.org/10.1175/1520-0442(2003)016<0571:BPOASF>2.0.CO;2, 2003.

Fetterer, F., K. Knowles, W. N. Meier, M. Savoie, and A. K. Windnagel. 2017, updated daily. *Sea Ice Index, Version 3*. Sea Ice Index, Version 3. Boulder, Colorado USA.

Deleted: Coachman, L. K.: Production of supercooled water during sea ice formation, Proceedings of the Symposium on Arctic Heat Budget and Atmospheric Circulation, Lake Arrowhead, California, 31 January–4 February 1966, 497–529, 1966.¶

Deleted: https://doi.org/10.1175/1520-0442(2003)016

NSIDC: National Snow and Ice Data Center. https://doi.org/10.7265/N5K072F8. 09 March 2019.

Fusco, G., Flocco, D., Budillon, G., Spezie, G., and Zambianchi, E.: Dynamics and variability of terra nova bay polynya, Marine Ecology, 23, 201–209, https://doi.org/10.1111/j.1439-0485.2002.tb00019.x, 2002.

Fusco, G., Budillon, G., and Spezie, G.: Surface heat fluxes and thermohaline variability in the ross sea and in terra nova bay polynya, Cont. Shelf Res., 29(15), 1887-1895. https://doi.org/10.1016/j.csr.2009.07.006, 2009.

Gallée, H.: Air-sea interactions over terra nova bay during winter: simulation with a coupled atmosphere-polynya model, J. Geophys. Res-Atmos., 102, 13835–13849, https://doi.org/10.1029/96JD03098, 1997.

Heorton, H. D. B. S., Radia. N., and Feltham, D. L.: A model of sea ice formation in leads and polynyas, J. Phys. Oceanogr., 47, 1701-1718, https://doi.org/10.1175/JPO-D-16-0224.1, 2017.

Ito, M., Ohshima, K., Fukamachi, Y., Simizu, D., Iwamoto, K., Matsumura, Y., . . . Eicken, H. Observations of supercooled water and frazil ice formation in an Arctic coastal polynya from moorings and satellite imagery, Ann. Glaciol., 56, 307-314, https://doi.org/10.3189/2015AoG69A839, 2015.

Jacobs, S. S.: Bottom water production and its links with the thermohaline circulation, Antarct. Sci., 16, 427-437, https://doi.org/10.1017/S095410200400224X, 2004.

Knuth, M. A. and Ackley, S. F.: Summer and early-fall sea-ice concentration in the ross sea: comparison of in situ ASPeCt observations and satellite passive microwave estimates, Ann. Glaciol., 44, 303-309, https://doi.org/10.3189/172756406781811466, 2017.

Kurtz, D. D. and Bromwich, D. H.: A recurring, atmospherically forced polynya in terra nova bay in Antarctic Research Series, 43, edited by: Jacobs, S.S., 43, American Geophysical Union,Washington, D.C., 177-201, https://doi.org/10.1029/AR043p0177, 1985.

Lombardo, C., and Gregg, M.: Similarity scaling of viscous and thermal dissipation in a convecting surface boundary layer., J. Geophys. Res., 94, , 6273-6284. https://doi.org/10.1029/JC094iC05p06273, 1989.

Formatted: Default Paragraph Font, Font: (Default) Arial, 11 pt

Deleted: Jones, D. W. R. and Wells, A. J.: Frazil-ice growth rate and dynamics in mixed layers and sub-ice-shelf plumes, The Cryosphere, 12, 25–38. https://doi.org/10.5194/tc-12-25-2018, 2018.¶

Deleted: https://doi.org/10.1029/AR043p0177

Deleted: https://doi.org/10.1029/JC094iC05p06273

Manwell, J. F., McGowan, J. G., and Rogers, A. L. Wind energy explained: theory, design and application. John Wiley & Sons, West Sussex, England, https://doi.org/10.1002/9781119994367, 2010.

Martin, S.: Frazil ice in rivers and oceans, Annu. Rev. Fluid Mech., 13(1), 379-397. https://doi.org/10.1146/annurev.fl.13.010181.002115, 1981.

Martin, S., Drucker, R. S., and Kwok, R.: The areas and ice production of the western and central ross sea polynyas, 1992-2002, and their relation to the B-15 and C-19 iceberg events of 2000 and 2002, J. Marine Syst., 68, 201-214, https://doi.org/10.1016/j.jmarsys.2006.11.008, 2007.

Mathiot, P., Jourdain, N., Barnier, C., Gallée, B., Molines, H., Sommer, J., and Penduff, M.: Sensitivity of coastal polynyas and high-salinity shelf water production in the Ross Sea, antarctica, to the atmospheric forcing, Ocean Dynam., 62(5), 701-723, https://doi.org/10.1007/s10236-012-0531-y, 2012.

Matsumura, Y., and Ohshima, K. I.:. Lagrangian modelling of frazil ice in the ocean, Ann. Glaciol., 56(69), 373–382, https://doi.org/10.3189/2015AoG69A657, 2017.

Michel, B.: Physics of snow and ice: morphology of frazil ice, International Conference on Low Temperature Science. I, Conference on Physics of Snow and Ice, II, Conference on Cryobiology, Sapporo, Japan, 14-19 August 1966, Sapporo, Japan, 119–128, 1967.

Monin, A. S., and Obukhov, A. M.: Basic laws of turbulent mixing in the surface layer of the atmosphere, Contrib. Geophys. Inst. Acad. Sci. USSR, 24, 163-187, 1954.

Morales Maqueda, M. A., Willmott, A. J., and Biggs, N. R. T.: Polynya dynamics: a review of observations and modeling, Rev. Geophys., 42(1), RG1004, https://doi.org/10.1029/2002RG000116, 2004.

Nelson, M., Queste, B., Smith, I., Leonard, G., Webber, B., & Hughes, K. (2017). Measurements of Ice Shelf Water beneath the front of the Ross Ice Shelf using gliders. Annals of Glaciology, 58(74), 41-50. doi:10.1017/aog.2017.34

Nihashi, S. and K.I. Ohshima: Circumpolar mapping of Antarctic coastal polynyas and landfast sea ice: relationship and variability. Journal of Climate, 28, 3650-3670, https://doi.org/10.1175/JCLI-D-14-00369.1 2015.

Orsi, A.H. and Wiederwohl, C.L.: A recount of Ross Sea waters, Deep-Sea Res. Pt. II, 56(13), 778-795, https://doi.org/10.1016/j.dsr2.2008.10.033, 2009.

Deleted: r

Deleted: s

Deleted: ,

Commented [TLML(23]: Unsure how to address

Commented [BL24]: Just add this caveat to the paragraph and include the citation. That "warns" the reader.

Formatted: Font: 12 pt

Deleted: r

Deleted: s

Ohshima, K.I., Nihashi, S. & Iwamoto, K. Global view of sea-ice production in polynyas and its linkage to dense/bottom water formation. Geosci. Lett. 3, 13, https://doi.org/10.1186/s40562-016-0045-4, 2016.

Ozsoy-Cicek, B., Xie, H., Ackley, S. F., and Ye, K.: Antarctic summer sea ice concentration and extent: comparison of ODEN 2006 ship observations, satellite passive microwave and NIC sea ice charts, The Cryosphere, 3(1), 1-9, https://doi.org/10.5194/tc-3-1-2009, 2009.

Park, J., Kim, H.-C., Jo, Y.-H., Kidwell, A., and Hwang, J.: Multi-temporal variation of the ross sea polynya in response to climate forcings, Polar Res., 37(1), https://doi.org/10.1080/17518369.2018.1444891, 2018.

Pease, C. H.: The size of wind-driven coastal polynyas. J. Geophys. Res., 92(C7), 7049-7059, https://doi.org/10.1029/JC092iC07p07049, 1987.

Petrelli, P., Bindoff, N. L., and Bergamasco, A.: The sea ice dynamics of terra nova bay and ross ice shelf polynyas during a spring and winter simulation, J. Geophys. Res.-Oceans, 113(C9), https://doi.org/10.1029/2006JC004048, 2008.

Robinson, N. J., Williams, M. J., Stevens, C. L., Langhorne, P. J., and Haskell, T. G.:Evolution of a supercooled ice shelf water plume with an actively growing subice platelet matrix, J. Geophys. Res.-Oceans, 119(6), 3425-3446, https://doi.org/10.1002/2013JC009399, 2014.

Robinson, N.J., Grant, B.S, Stevens, C.L., Stewart, C.L., Williams, M.J.M. Oceanographic observations in supercooled water: Protocols for mitigation of measurement errors in profiling and moored sampling, Cold Regions Science and Technology, 170, https://doi.org/10.1016/j.coldregions.2019.102954, 2019.

Sansiviero, M., Morales Maqueda, M. Á., Fusco, G., Aulicino, G., Flocco, D., and Budillon, G.: Modelling sea ice formation in the terra nova bay polynya, J. Marine Syst., 166, 4–25, https://doi.org/10.1016/j.jmarsys.2016.06.013, 2017.

SBE 911plus CTD- SBE 911plus CTD Datasheet: https://www.seabird.com/profiling/sbe-911plus-ctd/family-downloads?productCategoryId=54627473769, 15 August 2018, 2016.

Formatted: Default Paragraph Font, Font: (Default) Arial, 11 pt

Skogseth, R., Nilsen, F., and Smedsrud, L. H.: Supercooled water in an Arctic polynya: observations and modeling, J. Glaciol., 55(189), 43–52, https://doi.org/10.3189/002214309788608840, 2009.

Smith, M., and Thomson, J.: Ocean surface turbulence in newly formed marginal ice zones, J. Geophys. Res.-Oceans, 124(3), 1382-1398, https://doi.org/10.1029/2018JC014405, 2019.

Talley, L.D., Picard, G.L., Emery, W.J. Swift, J.H.: Descriptive physical oceanography: an introduction, 6, Academic Press, Elsevier, Boston, 2011.

Tamura, T., Ohshima, K. I., and Nihashi, S.: Mapping of sea ice production for antarctic coastal polynyas, Geophys. Res. Lett., 35(7), 1–5, https://doi.org/10.1029/2007GL032903, 2008.

Tamura, T., K. I. Ohshima, A. D. Fraser and G. D. Williams: Sea ice production variability in Antarctic coastal polynyas, J. Geophys. Res., 121, 2967- 2979, https://doi.org/10.1002/2015JC011537, 2016.

Thomson, J.: Wave breaking dissipation observed with "swift" drifters, J. Atmos. Ocean Tech.,, 29(12), 1866–1882, https://doi.org/10.1175/JTECH-D-12-00018.1, 2012.

Thomson, J., Schwendeman, M., and Zippel, S. Wave-breaking turbulence in the ocean surface layer., J. Phys. Oceanogr., 46, 1857–1870, https://doi.org/10.1175/JPO-D-15-0130.1, 2016.

Ushio S., and Wakatsuchi, M.: A laboratory study on supercooling and frazil ice production processes in winter coastal polynyas, J. Geophys. Res.-Oceans, 98(C11), 20321–20328, https://doi.org/10.1029/93JC01905, 1993.

Van Woert, M. L.: The wintertime expansion and contraction of the terra nova bay polynya, Oceanography of the Ross Sea: Antarctica, Spezie, G. and Manzella, G. M. R., Springer, Milano, 145-164, https://doi.org/10.1007/978-88-470-2250-8_10, 1999a.

Van Woert, M. L.: Wintertime dynamics of the terra nova bay polynya, J. Geophys. Res., 104, 7753-7769, https://doi.org/10.1029/1999JC900003, 1999b.

Vallis, G. (2017). *Atmospheric and Oceanic Fluid Dynamics: Fundamentals and Large-Scale Circulation.* Cambridge: Cambridge University Press. doi:10.1017/9781107588417.

Deleted: a

Formatted: Default Paragraph Font, Font: (Default) Arial, 11 pt

Formatted: Indent: Left: 0.33", Hanging: 0.33", Line spacing: 1.5 lines

Formatted

Weissling, B., Ackley, S., Wagner, P., and Xie, H.: EISCAM — Digital image acquisition and processing for sea ice parameters from ships, Cold Reg. Sci. Technol., 57(1), 49-60, https://doi.org/10.1016/j.coldregions.2009.01.001, 2009.

Wilchinsky, A. V., Heorton, H. D. B. S., Feltham, D. L., and Holland, P. R.: Study of the impact of ice formation in leads upon the sea ice pack mass balance using a new frazil and grease ice parameterization, J. Phys. Oceanogr., 45(8), 2025–2047, https://doi.org/10.1175/JPO-D-14-0184.1, 2015.

Worby, A. P., Geiger, C. A., Paget, M. J., Van Woert, M. L., Ackley, S. F., and DeLiberty, T. L.: Thickness distribution of antarctic sea ice. J. Geophys. Res. - Oceans, 113(C5), https://doi.org/10.1029/2007JC004254, 2008.

Zhang, G.: A further study on estimating surface evaporation using monthly mean data: comparison of bulk formulations, J. Climate, 10(7), 1592-1600, https://doi.org/10.1175/1520-0442(1997)010%3C1592:AFSOES%3E2.0.CO;2, 1997.

Zippel, S. F., and Thomson, J. (2016). Air-sea interactions in the marginal ice zone. Elementa Science of the Anthropocene, 4, 95, http://doi.org/10.12952/journal.elementa.000095, 2016.

8. ACKNOWLEDGEMENTS

The authors appreciate the support of the National Science Foundation through NSF Award Nos 1744562 (B. Loose, L. de Pace, URI); 134717 (S.F. Ackley, UTSA); 1341513 (E. Maksym, WHOI);1341725 (P.Guest, NPS); 1341606 (S. Stammerjohn and J. Cassano, U Colo). The authors appreciate the support of the University of Wisconsin-Madison Automatic Weather Station Program for the data set, data display, and information.

9. DATA AVAILABILITY

The data used in this publication are publicly available from the US Antarctic Program Data Center http://www.usap-dc.org/view/dataset/601192

10. AUTHOR CONTRIBUTIONS

LD prepared the manuscript including all analysis. MS and JT provided SWIFT data and guidance for upper ocean turbulence analysis. SS prepared and processed the PIPERS CTD data and provided water mass insights during manuscript preparation; SA lead the PIPERS expedition and supported ice interpretations. BL participated in PIPERS expedition, inferred possibility of frazil ice growth and advised LD during manuscript preparation.

11. COMPETING INTERESTS

The authors declare that they have no conflict of interest.

Deleted: "

Page 16: [1] Deleted Brice Loose 6/3/20 6:24:00 PM

Page 16: [2] Deleted Brice Loose 6/3/20 6:26:00 PM

Page 16: [3] Deleted Brice Loose 6/3/20 6:29:00 PM

Page 16: [4] Deleted Lisa De Pace 4/28/20 8:28:00 PM

Page 16: [5] Deleted Brice Loose 6/3/20 6:32:00 PM

Page 16: [6] Deleted Brice Loose 6/3/20 6:32:00 PM

Page 16: [7] Deleted Brice Loose 6/3/20 6:36:00 PM

Page 16: [8] Deleted Brice Loose 6/3/20 6:37:00 PM

Page 16: [9] Deleted Brice Loose 6/3/20 6:38:00 PM

Page 16: [10] Deleted Lisa De Pace 4/28/20 8:44:00 PM

Page 30: [11] Deleted Brice Loose 5/28/20 5:11:00 PM

Page 30: [12] Deleted Brice Loose 5/28/20 5:22:00 PM

Page 31: [13] Formatted Table Lisa De Pace 4/29/20 8:20:00 PM

Formatted Table

Page 31: [14] Formatted Lisa De Pace 4/29/20 8:20:00 PM

Font: Italic

Page 35: [15] Deleted Lisa De Pace 4/30/20 3:06:00 PM

Page 35: [15] Deleted Lisa De Pace 4/30/20 3:06:00 PM

Page 35: [15] Deleted Lisa De Pace 4/30/20 3:06:00 PM

Page 35: [15] Deleted	Lisa De Pace	4/30/20 3:06:00 PM

Page 35: [15] Deleted	Lisa De Pace	4/30/20 3:06:00 PM